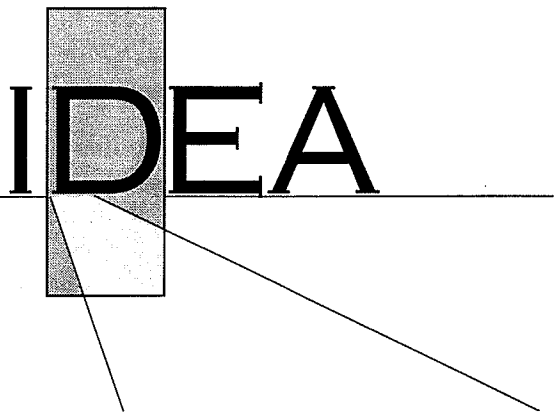

Innovations Deserving
Exploratory Analysis Programs

National Cooperative Highway Research Program

A NOVEL APPROACH TO DETERMINE MATERIAL PARAMETERS TO PREDICT REMAINING LIFE OF INFRASTRUCTURE

Final Report for NCHRP-IDEA Project 54

C.S. Desai, University of Arizona

November 2001

TRANSPORTATION RESEARCH BOARD • NATIONAL RESEARCH COUNCIL

INNOVATIONS DESERVING EXPLORATORY ANALYSIS (IDEA) PROGRAMS
MANAGED BY THE TRANSPORTATION RESEARCH BOARD (TRB)

This NCHRP-IDEA investigation was completed as part of the National Cooperative Highway Research Program (NCHRP). The NCHRP-IDEA program is one of the four IDEA programs managed by the Transportation Research Board (TRB) to foster innovations in highway and intermodal surface transportation systems. The other three IDEA program areas are Transit-IDEA, which focuses on products and results for transit practice, in support of the Transit Cooperative Research Program (TCRP), Safety-IDEA, which focuses on motor carrier safety practice, in support of the Federal Motor Carrier Safety Administration and Federal Railroad Administration, and High Speed Rail-IDEA (HSR), which focuses on products and results for high speed rail practice, in support of the Federal Railroad Administration. The four IDEA program areas are integrated to promote the development and testing of nontraditional and innovative concepts, methods, and technologies for surface transportation systems.

For information on the IDEA Program contact IDEA Program, Transportation Research Board, 500 5th Street, N.W., Washington, D.C. 20001 (phone: 202/334-1461, fax: 202/334-3471, http://www.nationalacademies.org/trb/idea)

PREFACE

The research in this report was supported by NCHRP-IDEA Grant No. 54 (Dr. Inam Jawed project director); it includes development of the methodology to predict the current stress-strain response of materials such as mortar and concrete which have undergone mechanical loading and environmental effects. The procedure is based on the integration of a nondestructive (Lamb wave) technique and the disturbed state concept (DSC) for constitutive modeling of engineering materials.

At this time, the results are based on one-dimensional mechanical testing and Lamb wave measurements on four compositions of mortar (as the simulation for concrete). The results are promising and show that the Lamb wave technique can be used with the DSC to predict the current stress-strain response, and also to develop procedures for the prediction of remaining life. Future research is needed to further validate the approach with multidimensional testing of concrete, and to design the field equipment to determine the remaining life of concrete (and other materials) in infrastructure systems.

TABLE OF CONTENTS

ABSTRACT

This report describes the experimental and analytical results for the development of a methodology for predicting the stress-strain response of simulated concrete (mortar) in infrastructure. Lamb wave analysis is used to predict material properties of mortar specimens, which are used in the initial research as a substitute for concrete. The mortar specimens are tested to measure their stress-strain response under uni-axial compression. The results of the nondestructive and mechanical stress-strain testing are correlated to develop the model based on the Disturbed State Concept (DSC), a unified approach for modeling material behavior. This model can allow evaluation of the deformation moduli, strength and degradation (damage) at a given state during the life of the material. This information can be used to design rehabilitation strategies. It can also lead to the development of new computer based equipment that can be used in the field for defining the remaining life. At this time, the research involved one-dimensional testing. The proposed methodology can, however, be extended and improved by conducting two- and three-dimensional testing of concrete specimens, along with laboratory and field validations.

INTRODUCTION

The deformation and strength properties of structural materials such as concrete, metals, and asphalt in engineering structures modify (usually deteriorate) due to fatigue, wear and tear under applied loads and environmental effects (temperature, chemical attack, weather, etc.). As a consequence, it may happen that after a certain period of service life, the structure requires evaluation of its current condition, and as necessary, design of rehabilitation based on the deformation moduli and strength left during the service life.

A number of field measurement techniques have been used to make an evaluation of the condition of a structure. Nondestructive techniques [1-7] are among the most commonly used.

These methods usually allow for the computation of elastic properties such as Young's Modulus from nondestructive testing (NDT) properties. However, most available techniques do not provide information on the existing state of stress that can allow calculation of reduced values of moduli, and the remaining strength. Since both the deformation and strength properties are needed in the design for rehabilitation, it is desirable to develop a methodology that can permit evaluation of the entire stress-strain response including deformation and strength components corresponding to the current condition.

REVIEW OF PREVIOUS RESEARCH

In the inspection of metal materials and structures, NDT is an accepted practice. Ultrasonic and radiographic techniques have been used for some time to locate damage in the material, and there are recognized national and international standards on their use [5]. On the other hand, NDT of concrete is technologically far behind NDT of steel because of the complications involved with particle size, inhomogeneity, and fabrication. Steel and other metals are formed at plants, which adhere to controlled standards of production, whereas concrete is largely placed and cured in the field using relatively unskilled labor.

One of the most popular and significant applications of NDT has been to find flaws and determine the size and shape of flaws inside of a material. This is typically done for metals (specifically welds in pipes/pressure vessels) to determine if manufacturing or fabrication processes are done satisfactorily. It is proposed here, that this methodology can be extended on a more global scale such that many flaws are detected by a single test over a significant length of the material. In typical flaw detection, the wavelength used may be quite small compared to the size of the flaw. This works well because the wave is reflected by the material-flaw interface (or the surface of the flaw). On a global scale, however, short wavelengths will be scattered by these flaws, and the resulting signal can be noisy and inconsistent. A wavelength, which is large

compared to the flaw size, is required to determine the *overall* effect of flaws in the material. In this way, microscopic flaws, such as micro-cracks, or small voids due to particle motion (slip and rotation) can be quantified. For example, flaw density or amount of damage may be determined and assigned a value. Since a material develops flaws (micro-cracks or voids) as it is loaded, and the damage (or disturbance) is a function of the amount of flawed (or broken) material, it follows that the disturbance can be determined from Lamb wave testing.

One difficulty of NDT and especially of NDT for concrete is the attenuation of the measured wave. Lamb waves and other guided waves do not attenuate as quickly as bulk waves, giving better and more consistent results over a distance in the material. In addition, it has been shown that bulk waves are not affected greatly by changes in stress-strain properties [8], whereas the current research shows that Lamb wave characteristics can be altered greatly by small changes in these properties.

For these reasons, Lamb wave technique has been chosen as the tool with which to measure the internal damage in the mortar material. By varying the angle and frequency of the incident wave, different Lamb modes can be generated; these different modes may be more sensitive to different types of flaws leading to a more complete detection of internal damage.

Whitcomb et. al. [9] performed a series of acoustic tests and concluded that ultrasonic waves with frequency up to 510 kHz will propagate through 10 cm of concrete 0.8 cm aggregate size, while a larger aggregate concrete requires a lower frequency to propagate the same distance. It is generally accepted that low frequency waves are required to propagate through granular materials because high frequency (short wavelength) waves are scattered by the aggregate matrix interfaces. The mortar of the experiment conducted here has a maximum aggregate size of about 0.40 cm, and therefore 500 kHz transducers were used. The wavelength of a 500 kHz wave traveling at 2 km/s is 0.40 cm.

NEW CONTRIBUTIONS

The notion that Lamb wave testing can be used to evaluate damage in concrete is a relatively new concept [10-13]. Although NDT has been used for many years, the current research is different in two major aspects. First, the experimental setup excites specific Lamb modes by controlling frequency and striking angle, and second, the research focuses on combining and integrating the NDT results with a powerful constitutive model to predict the current deterioration or damage state of the material. Previous methods (referenced above) involve evaluation only of elastic (stiffness) moduli and are not capable of providing realistic evaluation of the current condition including degree of failure, plastic deformation and degradation.

The objective of the research has been to develop a new and unique procedure for defining the entire stress-strain (pre and post peak) response during the life of structural materials, like concrete, based on results of NDT. In this manner, both the deformation and strength properties can be evaluated. The procedure developed herein integrates nondestructive (Lamb wave) techniques and the Disturbed State Concept (DSC) for constitutive modeling of materials; it is called the NDT-DSC method. The DSC is formulated and integrated with NDT for the characterization of the current state of the material; details of the DSC are given later. Measurements such as dispersion curves and attenuation for different frequencies are obtained from the Lamb wave technique. The mechanical properties such as the state of stress and elastic modulus are obtained from uni-axial compression tests on specimens of mortar. The nondestructive and mechanical data is correlated to develop the methodology for predicting the current state of the material.

The DSC is fundamental and mechanistic, and at the same time, it can be simplified for practical applications [14]. For instance, the DSC is hierarchical and as a result, various previous models such as elastic, elasto-plastic, elasto-visco-plastic, and continuum damage are available as special cases, depending on the specific material and user need.

Figure 1 shows a schematic of the stress-strain response of a material that is affected by mechanical forces and environmental effects. The elastic modulus, which represents the slope, E^i, of the unloading response is often used to compute deformation. The maximum or peak stress, σ^p, is often a basis for the strength used in design.

A brittle material like mortar or concrete under loading may experience microcracking sometime before the peak is reached. Increasing load may cause further microcracking. The microcracks form, grow, and coalesce to become distinct fractures leading to initiation of failure. At a point in the material of an engineering structure during its service life, the state of stress can be anywhere between the initial and failure states. The objective is to develop a method that can permit evaluation of the current condition (elastic modulus, peak stress, etc.) of the material from NDT measurements.

The DSC method allows for the evaluation of the current or observed state of stress (σ^a) on the basis of the knowledge of the material's initial (relative intact – RI) and ultimate (fully adjusted – FA) states. The current response is obtained by using the interpolation and coupling function, called the disturbance function. Hence, if the disturbance is defined from the NDT, the current stress, σ^a, and also the current modulus, E^a can be obtained, (Fig. 1). Details of the NDT, DSC and the procedure for predicting the stress-strain response are given later in the Material Model section.

This exploratory research can lead to the development of field equipment in which the Lamb wave measurements are input into the DSC model that is installed on a computerized set-up. Then the design parameters for the current state prediction can be obtained directly from the field equipment.

EXPERIMENTAL STUDY

Quasi-static (loading, unloading, reloading) tests were conducted on mortar specimens to

determine stress-strain response and elastic properties. Mortar is used in this initial research as a substitute for concrete. Four sets of samples were tested both nondestructively and mechanically. Sample sets I, II, and III are used to develop the framework and determine parameters for the material model. The test sample set IV is used for an independent verification of the model; it was not used to determine any of the parameters for the model. In order to simulate the disturbance (damage), which would result from years of environmental and mechanical loading, each set is made from different mortar mixtures (Table 1) with different strengths. Each sample set contains five samples.

Specimen Preparation

Typical sample dimensions are shown in Figure 2. A block of mortar for each sample set was poured and allowed to cure outdoors for 48 hours. Then the block was placed in a humidity room and cured for two weeks. The block was then removed from the curing room and the samples were cut from it. Two strain gauges were attached to each sample; one in the axial direction, and one in the lateral direction (only axial was used for Sample set IV because the Poisson's ratio does not vary significantly, Table 2). The strain gauges measured 30 mm (~1.25 in) long, and were glued to the specimens using a fast drying epoxy. The epoxy was allowed to cure for 24 hrs before any testing was performed; in no case did the strain gauge de-bond from the sample. The samples were capped with a ceramic called hydrostone to give them a smooth flat hard surface.

Mechanical Test Procedure

All tests were displacement controlled. The test setup is shown schematically in Fig. 3. Each sample was loaded to peak with unloading at various points (displacement intervals) The loading continued until the samples could no longer support a nominal load.

Nondestructive Test Procedure

The nondestructive testing was performed with a Wavetek 100 MHz Arbitrary Waveform Generator (Model 395) controlled by a PC. Transducers were used in an immersed pitch-catch arrangement. The computer served as both the control and data acquisition devices, Fig. 4. The Wavetek generated signal was amplified before exciting the transducer, and the received signal was filtered before entering the computer (A/D converter).

The NDT samples were subjected to Lamb wave frequency sweep testing. The transducers used had a central frequency of 500 kHz, and a frequency scan was performed in order to plot the Amplitude vs. Frequency (V(f)) curves. The striking (incident) angle, θ, was held constant at 30°, Fig. 5. The range of the scan was between 100 kHz and 800 kHz for all samples.

Mechanical Test Results

Details of both mechanical and nondestructive testing are given in Appendix 1. The results of the mechanical tests are shown in Table 2; some data from sample set III is not shown because the samples exceeded the capacity of the testing device. The three mixtures cover a wide range of peak strengths; the average values are reported for each set of samples. The parameters A and Z are used in the DSC to define degradation and to predict the stress-strain responses, and will be discussed in more detail in the Material Model section.

Nondestructive Test Results

Figure 6 shows the V(f) curve for a typical sample; the amplitude or voltage, V, is plotted against the frequency, f. The computer is used to generate a signal at a frequency interval over the desired range. For the current research, the frequency interval is 4 kHz, and the range is from 100 kHz to 800 kHz. Three significant parameters are measured from the V(f) curve, the number

of peaks, the maximum peak value and the area under the curve. For the sample shown, the number of peaks is six, the maximum peak value is approximately 10 V, and the area under the curve is approximately 2500 V-Hz. The units for the maximum peak value, and the area under the curve are V and V-Hz respectively, but will be omitted intentionally to avoid confusion. For simplicity, Λ is defined as the area under the V(f) curve, which is an indirect measure of the transmitted energy. The maximum peak value is also an indirect measure of the transmitted energy, and therefore, the results of these two parameters should be very similar. The transmitted energy is a function of the attenuation of the material, and is therefore affected by the presence of micro damage in the material as well as the amplification of the system, and the distance of travel of the wave in the specimen. Unfortunately, the system amplification would vary from one test setup to another, and would be difficult to control in the field application of this method. The third parameter however, the number of peaks, is dependent only on the elastic properties of the material, and may be a more robust method of predicting the stress-strain response. A more detailed explanation of this prediction method is given in the Discussion of Test Results section.

Table 2 and Fig. 7 summarize the results of the nondestructive testing; the parameters shown in Fig. 7 are normalized for comparison (each value is divided by the maximum value). The average values of the number of peaks, the maximum peak value, and the area under the V(f) curve, Λ, are given for each mortar mixture.

Discussion of Test Results

A number of observations can be made from Fig. 7: (1) The number of peaks detected decreases with an increase in strength of the mortar, (2) the maximum peak value increases with an increase in strength, and (3) the area under the V(f) curve, Λ, increases with an increase in strength.

Since the weaker mixtures are used to simulate the disturbance (damage), the test results

indicate that as the material experiences damaging effects, the number of peaks increases, and the maximum peak value and Λ decrease. It follows then, that a value of damage or disturbance, can be assigned to each mixture such that a correlation can be made between the NDT measurements, and the disturbance of the specimen. With this correlation defined, it is then possible to independently predict the peak stress and other parameters for any mixture using the NDT measurements. The method of correlation and independent prediction are given later.

Lamb Wave Theory in Testing

The theory of Lamb waves states that waves propagating in a flat plate free on both top and bottom surfaces will propagate at discrete frequency intervals determined by the solutions of equations 1a and 1b [15, 16].

$$\frac{\tanh(\beta h)}{\tanh(\alpha h)} = \frac{4k^2\alpha\beta}{(k^2+\beta^2)^2} \quad \text{(symmetric modes)} \tag{1a}$$

$$\frac{\tanh(\beta h)}{\tanh(\alpha h)} = \frac{(k^2+\beta^2)^2}{4k^2\alpha\beta} \quad \text{(asymmetric modes)} \tag{1b}$$

where $\alpha = (k^2-k_p^2)^{.5}$, $\beta = (k^2-k_s^2)^{.5}$, and $k_s = \omega/c_s$, $k_p = \omega/c_p$, $k = \omega/c$, ω = frequency, c_s = shear wave velocity, c_p = compressional wave velocity, c = Lamb wave velocity, and h = plate thickness.

The derivation of these equations can be found in the literature. Although the solution to these equations is quite complex and typically requires numerical methods, the stress-strain response can be predicted without solving these equations. Figure 8 shows the solutions to Eqs. (1) over a range of frequencies for an intact, and a damaged thin mortar plate (only symmetric modes are shown for clarity). These curves give the phase velocity of the wave in terms of the excitation frequency, and are called the dispersion curves. The velocity of the transmitted wave

is determined by Snell's law

$$\frac{V_i}{\sin(\theta_i)} = \frac{V_t}{\sin(\theta_t)} \tag{2a}$$

where V_i is the velocity of the incident wave, V_t is the velocity of the transmitted wave, θ_i is the incident angle (measured from a line perpendicular to the surface of the sample), and θ_t is the angle of the transmitted wave. For Plate waves generated using immersion techniques, V_i is the longitudinal wave speed in water (1.49 km/s), and the angle of the transmitted wave is 90°. This simplifies the equation to

$$V_t = \frac{1.49\ km\ /\ s}{\sin(\theta)} \tag{2b}$$

For an incident angle of 30°, the Lamb wave phase velocity is about 3 km/s as shown in Fig 8. Comparison of Figs. 8a and 8b reveals that a damaged sample can propagate many more Lamb modes over a given frequency range than an intact plate. Therefore, the V(f) scan, Fig 5, for a damaged plate should show more peaks over a specific frequency range than an intact plate. The NDT results, Fig 7, also show this trend. Therefore, the number of peaks can be used to predict the damage state of the material. The amplification of the system, and the attenuation of the material can be ignored giving this method a clear advantage over methods which rely on the amplitude.

MATERIAL MODEL

Numerous constitutive models exist today for the characterization of the three-dimensional stress-strain behavior of materials. Many of these models are complicated and relate only to

specific features of material behavior such as elastic, plastic or damage. The Disturbed State Concept (DSC) requires the definition of two material responses called reference states, and only one parameter called the disturbance. It is a unified, yet simplified approach for the characterization of significant features such as elastic, plastic, and creep strains, microcracking, damage, and softening, in a single framework [14]. Comparisons of the DSC with other models, (such as damage, fracture, and micromechanical) together with its advantages in terms of generality and simplification for practical use are given by Desai [14].

The DSC is based on the idea that a deforming material is composed of relative intact (RI) or continuous and fully adjusted (FA) parts. The FA parts are due to cracking, and particle slippage, rotations, etc. [14]. The DSC defines the exhibited behavior in terms of the responses of the RI and FA parts through a coupling and interpolation function called the disturbance function.

The RI state can be defined in a number of ways. It can be defined, for example, as the linear elastic response neglecting microcracks (Fig. 1) or it may be defined as the elasto-plastic behavior neglecting friction, which would cause loss of energy. A constitutive model such as the δ_o version in the hierarchical single surface (HISS) concept is often used to represent the RI state [14], which includes irreversible or plastic deformations. The relative intact response is relative in the sense that it excludes the effect of factors, which would cause the material to deviate from its initial intact state. Therefore, the choice of the constitutive model to define the RI state that will allow characterization of the necessary material parameters will depend on the type of material and laboratory data.

As the material is loaded, (i.e. loaded, unloaded, etc.) parts of the material may change from the RI state to the FA state. The location and amount of the FA portions of the material will depend on the initial state of the material, residual stresses, flaws, discontinuities, and microcracking. At the local level, the material particles may experience instantaneous instability and move (e.g. translation and rotation movements are possible). The measured response at the

macro level will integrate all of the material responses at the micro level to give an overall behavior, which can be modeled using the DSC. The FA material can be characterized in a number of ways. If it is considered to be a constrained liquid-solid (constrained by the RI material), then it may be able to resist both shear and normal stresses. If the FA material is considered to be like a constrained liquid, then it will only be able to resist normal stresses, and will have no shear strength. Finally, if it is considered to be a crack or void, then it has zero strength and can not resist shear or normal stresses (which is consistent with the assumption in the classical damage model [17]). Note that this allowance for an FA state by the DSC model is very important, and is what sets this model apart from classical damage models. The assumption that damaged material carries no stress at all may be valid at or near failure, however, the effect of the damaged portions of a material on its stress-strain behavior is generally significant. The disturbance function allows for this effect, and also for the effect of interaction between the FA and the RI portions. For the current research, the FA behavior is assumed to be a constrained liquid solid, and is defined as a small constant stress for any strain.

For the general three-dimensional case, the constitutive equations with disturbance are formulated from [14]:

$$\sigma_{ij}^{a} = (1-D)\sigma_{ij}^{i} + D\sigma_{ij}^{c} \tag{3}$$

where σ_{ij} is the stress tensor, the superscripts i, a, and c correspond to the RI, observed, and FA behaviors respectively, and D is the disturbance assumed to be a scalar in a weighted sense, Fig 1. The incremental form of Eq. (3) is given by

$$d\sigma_{ij}^{a} = (1-D)\sigma_{ij}^{i} + D\sigma_{ij}^{c} + dD(\sigma_{ij}^{c} - \sigma_{ij}^{i}) \tag{4a}$$

or

$$d\sigma_{ij}^{a} = (1-D)C_{ijkl}^{i}d\varepsilon_{kl}^{i} + DC_{ijkl}^{c}d\varepsilon_{kl}^{c} + dD(\sigma_{ij}^{c} - \sigma_{ij}^{i})$$

(4b)

where C_{ijkl} is the constitutive tensor and dD is the increment or rate of disturbance. The one-dimensional specialization of Eq. (3) is given as

$$\sigma^a = (1-D)\sigma^i + D\sigma^c \tag{5}$$

Similarly the observed elastic, E, and shear, G, moduli can be expressed in terms of the disturbance as, [14]

$$E^a = (1-D)E^i + DE^c \tag{6}$$

$$G^a = (1-D)G^i + DG^c \tag{7}$$

Alternatively, the disturbance may be expressed in terms of stress or elastic modulus as

$$D_\sigma = \frac{\sigma^i - \sigma^a}{\sigma^i - \sigma^c} \tag{8a}$$

$$D_E = \frac{E^i - E^a}{E^i - E^c} \tag{8b}$$

where E^a denotes observed modulus at a given state, Fig 1. Using Eq. (8a), the disturbance can be calculated at any point on a measured stress-strain response. The plastic strain can also be calculated at any point from

$$\varepsilon_p = \varepsilon - \frac{\sigma^a}{E} \tag{9}$$

where ε is the total strain, ε_p is the plastic strain, σ^a is the observed stress, and E can be assumed to be the initial elastic modulus. A plot of disturbance vs. elastic and plastic strain for a typical sample (I-4) is shown in Fig. 9. It is clear that the disturbance and the plastic strain are related, i.e. both are measurements of damage. If the plastic strain is zero, the disturbance is also zero, and disturbance values close to 1.0 imply that nearly all of the strain is plastic. In order to predict the stress-strain response, a relation between disturbance and plastic strain is required. Figure 9 suggests that the disturbance can be approximated as an exponential function of the plastic strain in the form

$$D = D_u(1 - e^{-A\varepsilon_p^Z}) \tag{10}$$

where D_u is the ultimate disturbance (usually 1.0), ε_p is the plastic strain, and A and Z are constants to be defined. Rearranging Eq. (10) into the slope intercept form gives

$$y = Zx + \ln(A) \tag{11}$$

where $y = \ln(-\ln(1-D/D_u)$, and $x = \ln(\varepsilon_p)$. Figure 10 shows a plot of y vs. x for a typical sample (I-4). The constants Z and A are now determined from the slope and intercept of this regression line, and are assumed to be material constants. Substituting ε_p from Eq. (9) into Eq. (10) and then substituting D from Eq. (10) into Eq. (5), gives an implicit relation between the observed stress and the total strain in the form

$$\sigma^a = \left(1 - D_u\left(1 - e^{-A\left(\varepsilon - \frac{\sigma^a}{E}\right)^Z}\right)\right)\sigma^i + D_u\left(1 - e^{-A\left(\varepsilon - \frac{\sigma^a}{E}\right)^Z}\right)\sigma^c \tag{12}$$

where σ^i and σ^c are the RI and FA stresses respectively. For the current research, an exponential function of the following form is used to define the RI behavior,

$$\sigma^i = \frac{E}{B}\left(1 - e^{-B\varepsilon}\right) \tag{13}$$

where $E = E^i$ is the initial elastic modulus, $B = E/(2\sigma^p)$ and σ^p = peak stress. The FA behavior is defined as a small constant value of stress, 10 psi. Substituting Eq. (13) into Eq. (12) gives

$$\sigma^u = \left(1 - D_u\left(1 - e^{-A\left(\varepsilon - \frac{\sigma^a}{E}\right)^Z}\right)\right)\frac{E}{B}\left(1 - e^{-E\varepsilon}\right) + D_u\left(1 - e^{-A\left(\varepsilon - \frac{\sigma^a}{E}\right)^Z}\right)\sigma^c \tag{14}$$

which can be solved numerically to back predict the stress-strain response, Fig. 11.

It is clear that the DSC can back predict the stress-strain response satisfactorily, but the true value of the NDT-DSC method is in the independent predictions, which are possible from the nondestructive testing. Combining the results of the Lamb wave analysis with the power of the disturbed state concept leads to a very useful tool in predicting the stress-strain response of a material. This tool is described next.

CORRELATION BETWEEN DSC AND NONDESTRUCTIVE BEHAVIOR FROM LAMB WAVE MEASUREMENTS

The disturbance, D, due to the mechanical and environmental loading will change, usually increase, in time. In the subsequent research, it can be defined from tests (mechanical and

nondestructive) based on measurements in which the loads and environmental effects are simulated in the laboratory. Thus far, the disturbance parameter and the DSC have been used to back predict the stress-strain responses and to find the parameters A and Z using the assumed RI and FA behavior defined previously. If a relation between the disturbance parameter and the NDT measurements can be found, then the Lamb wave results can quantify the disturbance, and the DSC can predict the current state of a material and its stress-strain response.

Let Λ equal the area under the V(f) curve as defined in the Experimental Study section. It is known that an intact specimen will transmit more energy than a damaged or broken specimen. Because Λ is an indirect measure of the transmitted energy, it stands to reason that it can be used to define the disturbance. Since values of Λ are known for each damaged state (each mixture), the values of disturbance can be calculated from

$$D = \frac{\Lambda^i - \Lambda^a}{\Lambda^i - \Lambda^c} \tag{15a}$$

where the initial and final values, Λ^i and Λ^c, are adopted based on test results. Mixture I was intentionally made very weak so that it is considered to be close to the FA state of the material, and mixture III was made very strong so that it is considered to be close to the RI state of the material. It can be assumed, then, that the disturbance of mixture I, and that of mixture III are approximately $D_I = 0.99$, and $D_{III} = 0.01$. Substitution of these values and the values of Λ (Λ^a) from Table 2 gives

$$0.99 = \frac{\Lambda^i - 48133}{\Lambda^i - \Lambda^c} \tag{16a}$$

$$0.01 = \frac{\Lambda^i - 2711424}{\Lambda^i - \Lambda^c} \tag{16b}$$

Solving Eqs. (16) for Λ^i and Λ^c gives

$$\Lambda^i = 2{,}738{,}600 \text{ mV-Hz}$$

$$\Lambda^c = 20{,}957 \text{ mV-Hz}$$

The disturbance of mixture II can then be defined from Eq. (15a), with $\Lambda^a = \Lambda_{II} = 868567$, giving $D_{II} = 0.69$. The disturbance can also be calculated from the max peak, P, or the number of peaks, #p, using Eq. (15b) and (15c), respectively.

$$D = \frac{P^i - P^a}{P^i - P^c} \tag{15b}$$

$$D = \frac{\#p^i - \#p^a}{\#p^i - \#p^c} \tag{15c}$$

Now, a value of disturbance has been defined for each mixture. The average values of disturbance calculated from Λ and the peak stress for the different mixtures are plotted in Fig. 12. Linear regression is used to fit a line to the data, and the equation of this line is given by Eq. (5) as

$$\sigma_p = (1 - D)\sigma_p^i - D\sigma_p^c \tag{17a}$$

where σ_p is the peak stress and σ_p^i and σ_p^c are the corresponding RI and FA stresses respectively. Then the slope intercept form, Eq. (17a) is written as

$$\sigma_p = (\sigma_p^c - \sigma_p^i)D + \sigma_p^i \tag{17b}$$

where the values of slope and intercept are given in Fig. 12. Here the value of σ_p can represent the changing strength due to environmental and mechanical loading. Then for any value of disturbance, defined from the NDT parameter, the value of peak stress can be found from Eqs. (17). Similarly, the elastic modulus, E, and shear modulus, G, can be found by using the same procedure with Eqs. (6) and (7), and the parameters A and Z can be found using Eqs. (18) and (19) below

$$\ln(A^a) = (1-D)\ln(A^i) + D\ln(A^c) \tag{18}$$

$$Z^a = (1-D)Z^i + DZ^c \tag{19}$$

The natural log of A must be used because the parameter varies greatly from one damage state to another. Figures 13 and 14 show the variations of some measured mechanical and NDT parameters with disturbance calculated from Λ. It is clear that the only parameter which does not match a liner approximation closely is the elastic modulus, E; this is expected because E is traditionally expressed as a nonlinear function of peak stress. Therefore, Eqs. (6) and (7) may need some modification, but for the current research, they are assumed to be adequate.

It should be noted that the assumed values of disturbance, i.e. $D_I = 0.99$ and $D_{III} = 0.01$, are arbitrary and do not affect the predicted values. Equation (17b) shown in Fig. 12 will change if these values are different, but the relation between Λ and disturbance will also change proportionately, so that the predicted value of peak stress is the same.

Comment

Finally, it may be desirable to establish the correlation between the mechanical and NDT parameters (such as Λ) by measuring them at various states during the stress-strain behavior.

This objective can be performed in further research.

PREDICTIONS OF STRESS-STRAIN BEHAVIOR FROM FIELD NDT MEASUREMENTS

To verify the method described in the previous section independently, samples from mortar mixture IV were tested nondestructively and the parameters were predicted, Table 3. Then the stress-strain testing was conducted. The Λ value for mortar mixture IV is Λ_{IV} = 153,261 mV– Hz, then the disturbance calculated from Eq. (15a) is approximately D_{IV} = 0.95. From Eq. (17), Fig. 12, the predicted value of peak stress is 5.80 Mpa (841 psi). This compares well with the measured value of 5.74 Mpa (832 psi). Similarly, the values of E, A and Z were predicted from Eqs. (6), (18), and (19) respectively, and the results are given in Table 3. Using the parameters A and Z shown in Table 3, the stress-strain graph of mixture IV has been predicted using each of the three NDT parameters (# peaks, max peak, Λ) and Eq. 14. The results are shown in Fig. 15. It is clear that prediction using the max peak parameter yields a significantly higher peak stress than the other two methods, but all methods predict the elastic modulus, and the softening curve very well. However, the prediction based on Λ yields the best results.

ACHIEVEMENTS AND FUTURE RESEARCH

The foregoing results show that the stress-strain response of a material (mortar) can be predicted on the basis of the NDT measurements, e.g. Λ. Thus, the procedure is useful for the estimation of the stress-strain response and design parameters for rehabilitation and/or new construction of an infrastructure using only NDT measurements in conjunction with the laboratory correlation between NDT and stress-strain data.

The results are considered to be very promising, but further research is required before this method can be applied fully to field problems and situations; some factors are not considered in

this preliminary study in order to conduct initial research and show feasibility. Particularly, realistic samples such as bridge decks are significantly larger than the test samples. A more sensitive receiver or more powerful transmitter will probably be required. In addition, the tests should be expanded to include multi-axial loading of specimens made of concrete, which have larger aggregate size and may reflect longer wavelengths. The tests may also be expanded to measure the NDT parameters at different stages of the mechanical loading, i.e. test mechanically and nondestructively at the same time. Then a better correlation may be established between mechanical and NDT results.

FIELD EQUIPMENT

The method explained here lends itself most readily to the examination of bridge decks and other structures, which are flat, relatively thin, and composed of concrete/mortar material. Since Lamb waves are considered plate waves, and only propagate through a medium with two parallel interfaces, the NDT method may need to be modified for arbitrarily shaped structures. The research outlined here can lead to the development of field equipment to examine these types of structures, predict stress-strain responses, and evaluate design parameters for rehabilitation - all in the field. A schematic representation of this equipment called the Lamb Wave-DSC (LW-DSC) is presented in Fig. 15. An outline of the procedure, which would be carried out by this equipment, is given as follows:

1. Define RI and FA behavior, i.e. determine reference material parameters, e.g. (A^i, A^c, Z^i, Z^c) – these may be assumed or calculated based on the available or measured stress-strain behavior. Once known, these values can be considered material properties such as E or ν.
2. Define one or more of the reference NDT parameters, i.e. # peaks, max peak, Λ, for each reference state. These values may also be considered material properties.
3. Using the field equipment, measure the corresponding NDT property in the structure to

be evaluated, and calculate the value of disturbance using Eqs. (15).

4. Formulate disturbance function in terms of plastic strain using A and Z, Eq. (10).
5. Use Eq. (12) to predict the stress-strain response, as in Fig. 15.
6. The predicted values such as E, σ_{max} and degradation (disturbance) can be used to design rehabilitation strategies.

SUMMARY AND CONCLUSIONS

From the analysis presented herein, the following conclusions can be made

1. A Lamb wave frequency scan is capable of detecting the disturbance inside a thin mortar plate.
2. The information produced by the scan can be used in a number of ways to quantify internal damage or disturbance of the material.
3. The Disturbed State Concept (DSC) can be used in combination with the NDT data to predict the stress-strain response of damaged samples under mechanical and environmental loading.
4. The prediction is accurate enough that the predicted values can be used in the rehabilitation design of the structure.

In the exploratory stages, the combination of Lamb wave testing of concrete type materials, and the DSC has shown to be a powerful tool. With further research and development, portable equipment may be designed to predict the entire stress-strain response of bridge decks or other similar structures in the field.

ACKNOWLEDGEMENTS

A part of the research in this paper was supported by the IDEA project No. NCHRP-54 funded by the Federal Highway Administration (FHWA).

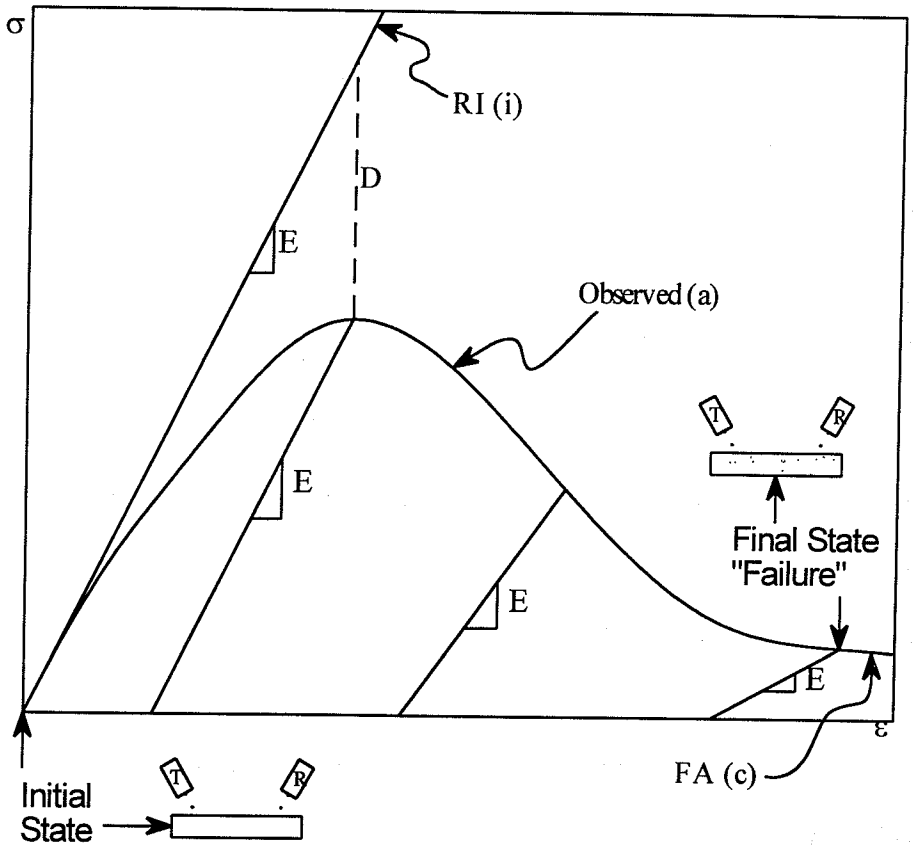

Figure 1—Schematic of stress-strain response. NDT-DSC concept

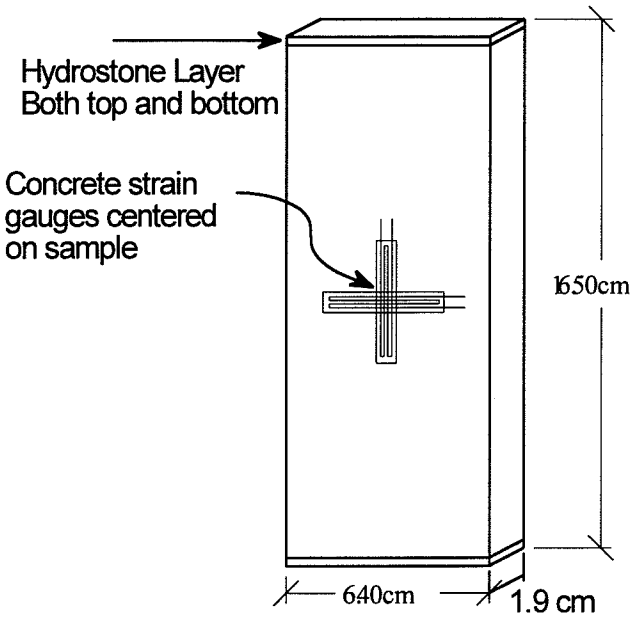

Fig. 2—Sample dimensions and preparation

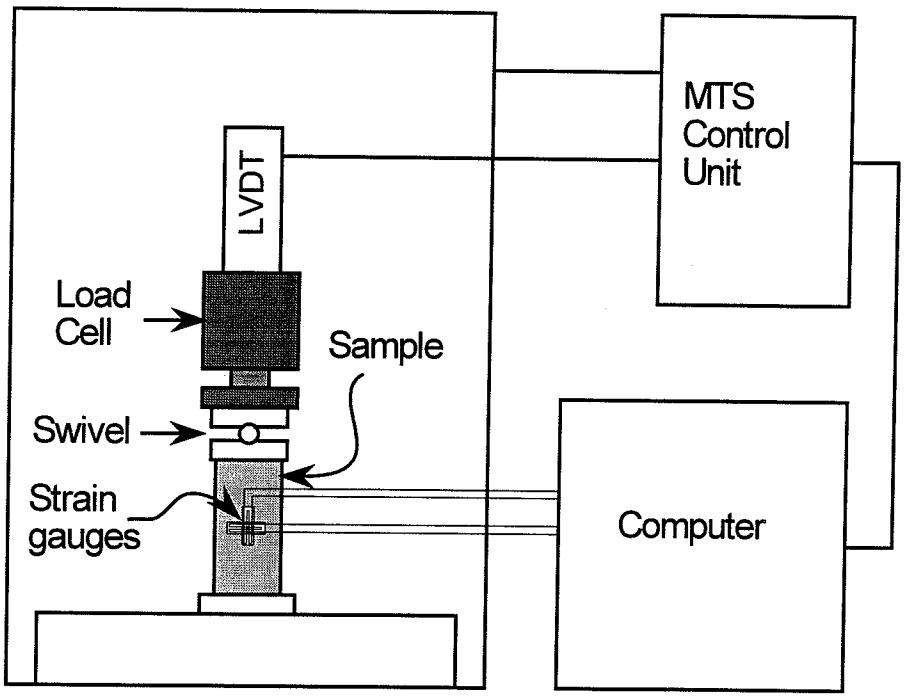

Fig. 3—Mechanical test setup

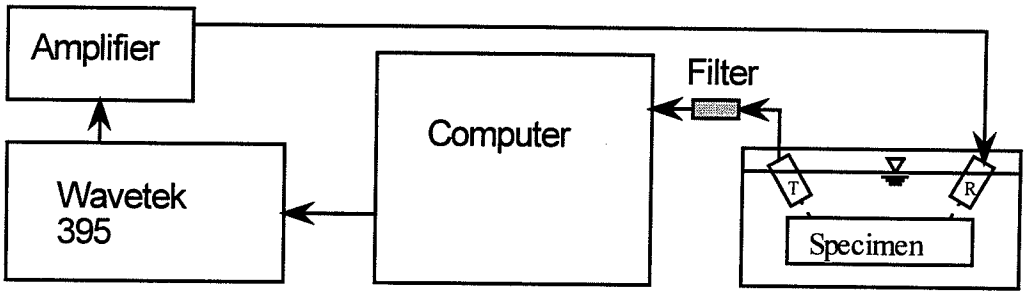

Fig. 4—Non Destructive Testing (NDT) setup

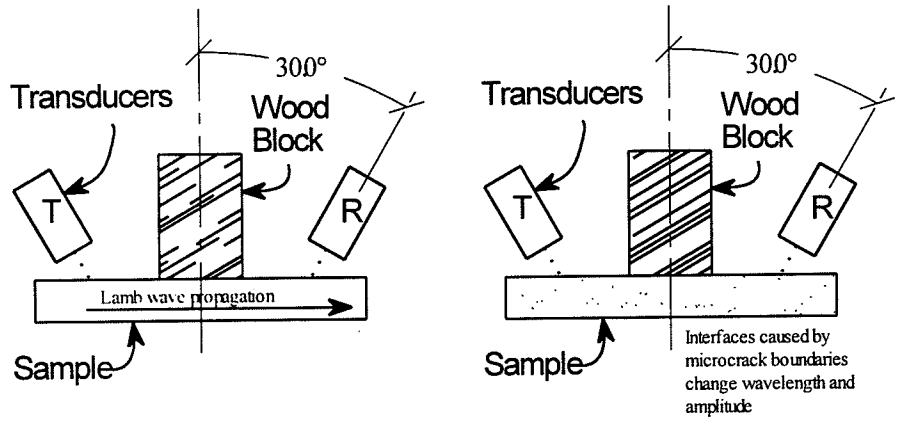

Fig. 5—Nondestructive testing setup and schematic of how damage affects Lamb wave propagation

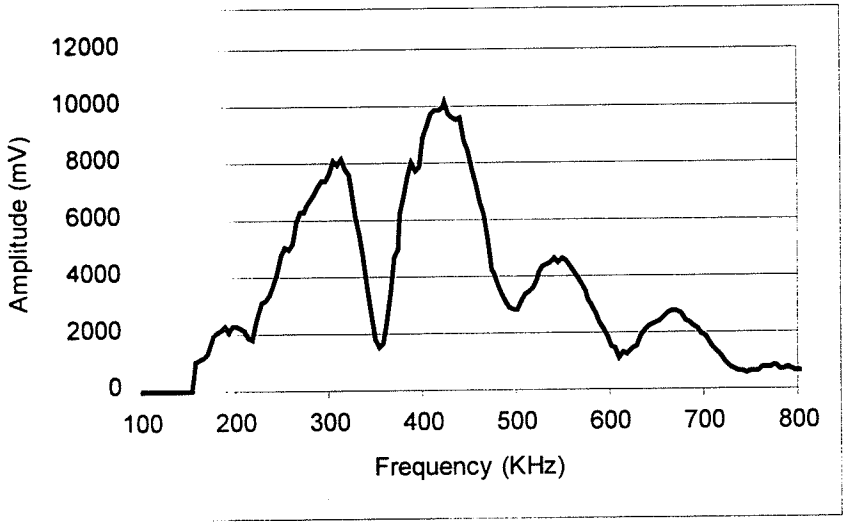

Fig. 6—V(f) curve for sample III-3

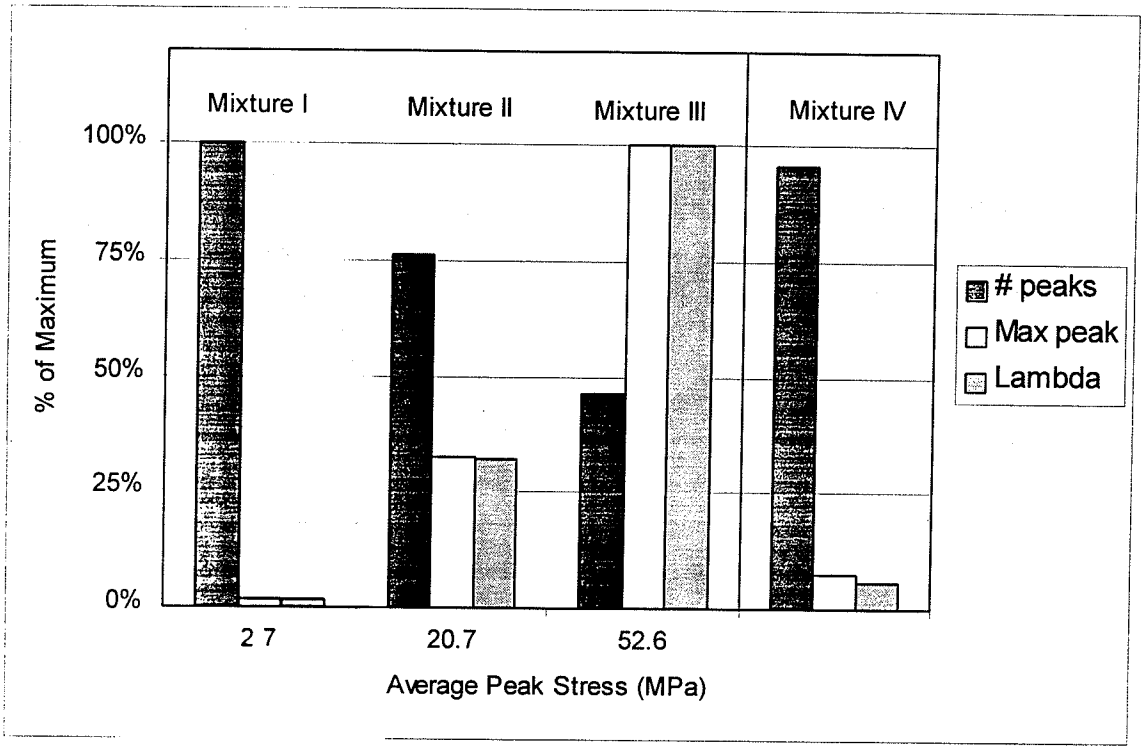

Fig. 7—Results of NDT

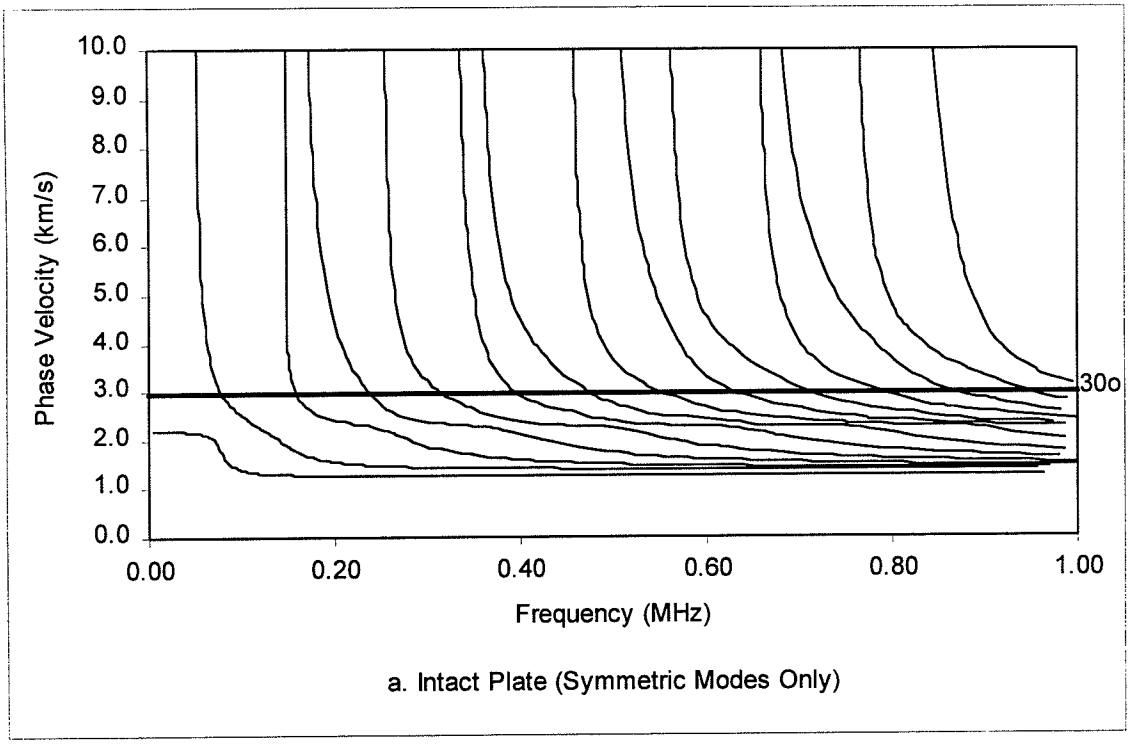

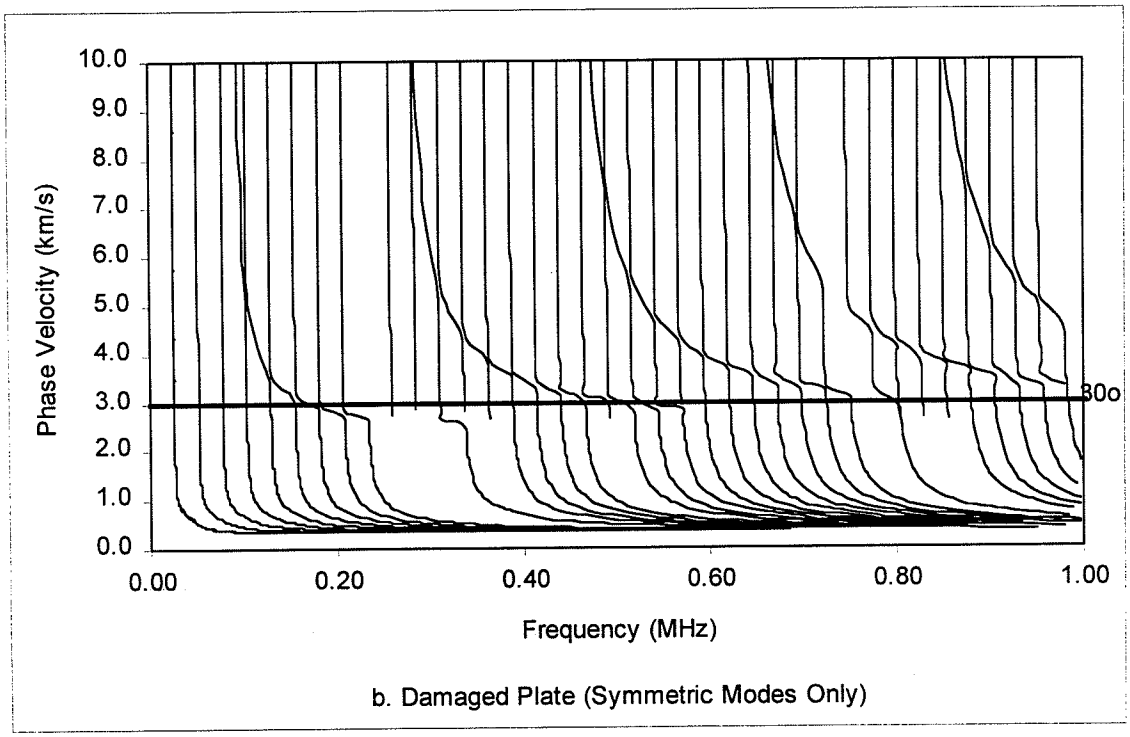

Fig. 8—Theoretical dispersion curves for a) intact and b) damaged thin mortar plate. 30° incident angle corresponding to phase velocity of 3 km/s. Each line represents a propagation mode.

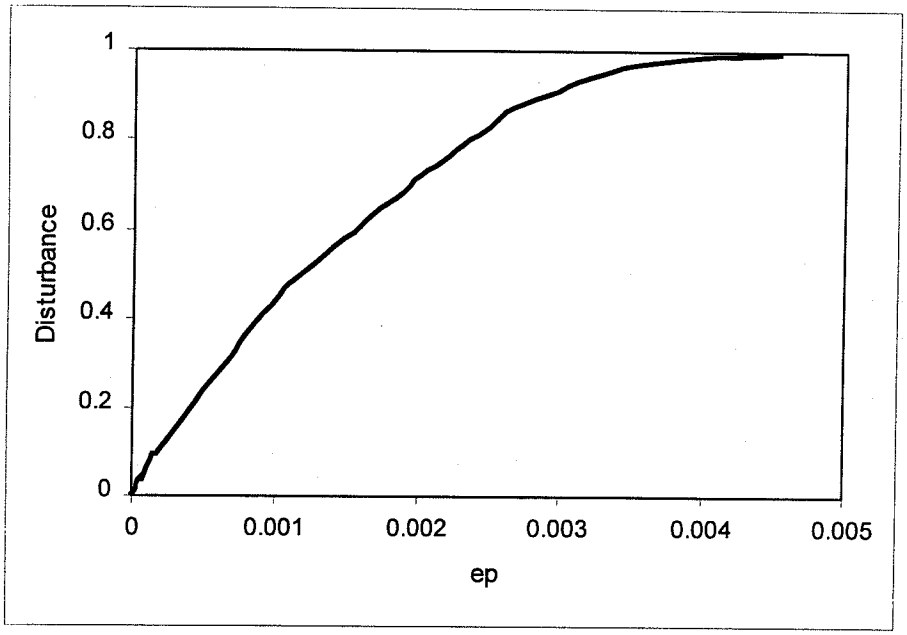

Fig. 9—Disturbance vs. plastic strain, Sample I-4

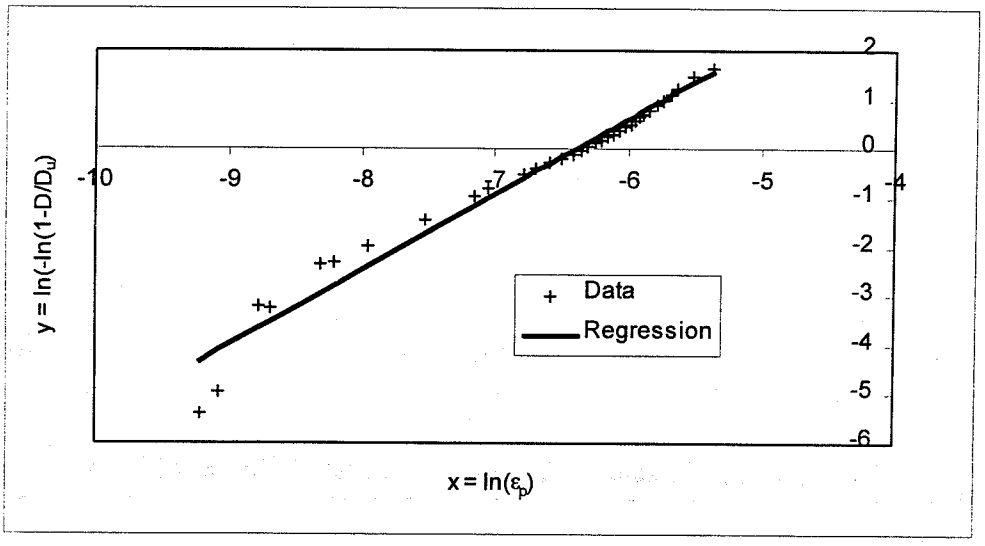

Fig. 10—Determination of parameters A and Z, sample I-4

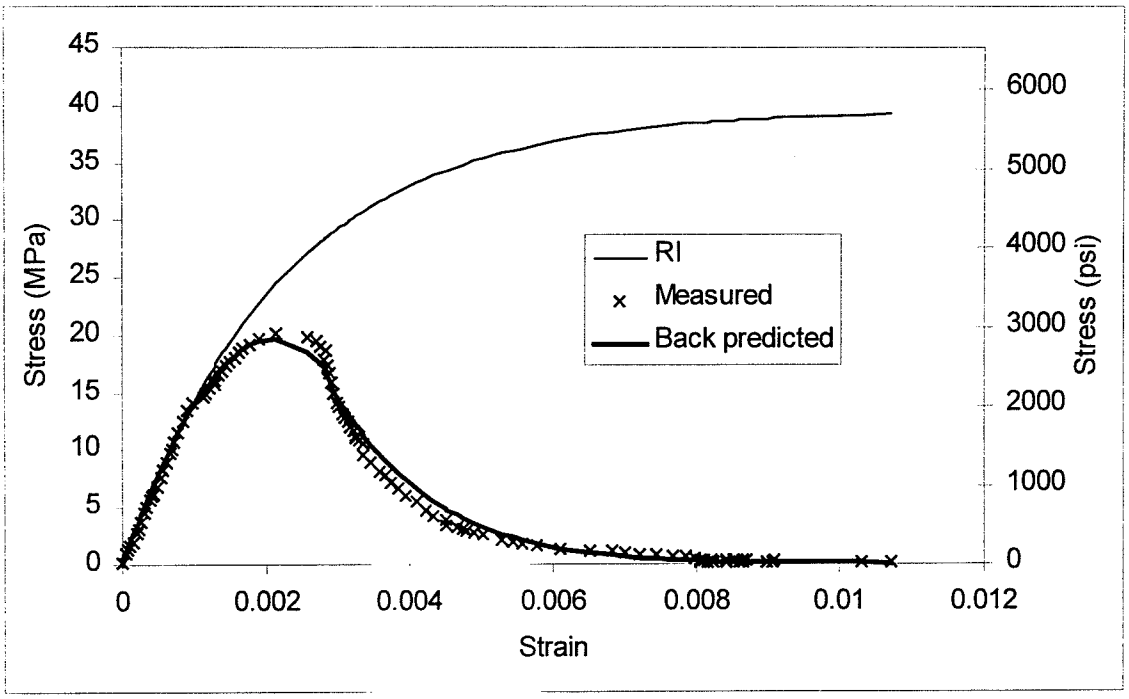

Fig. 11—Predicted response of Sample II-2

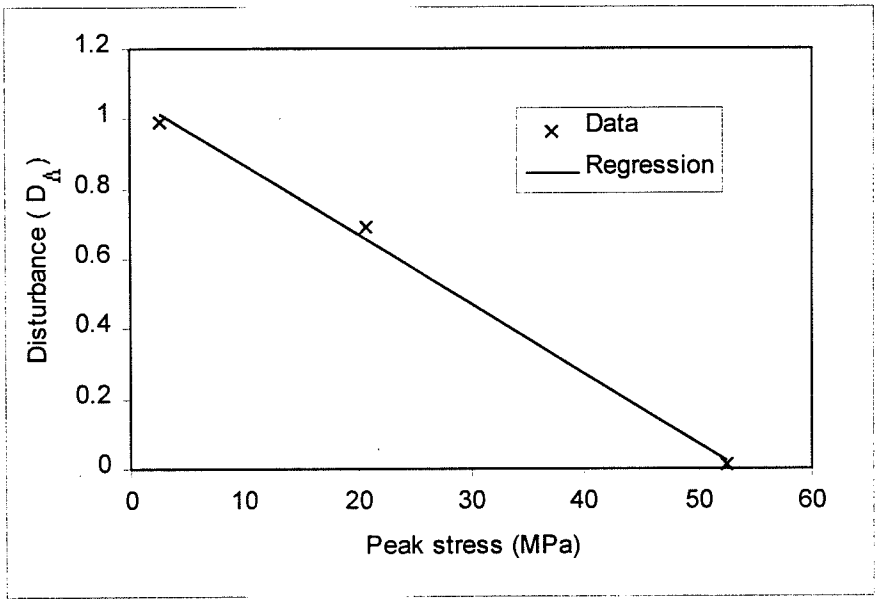

Fig. 12—Disturbance (from Λ) vs. peak stress and regression

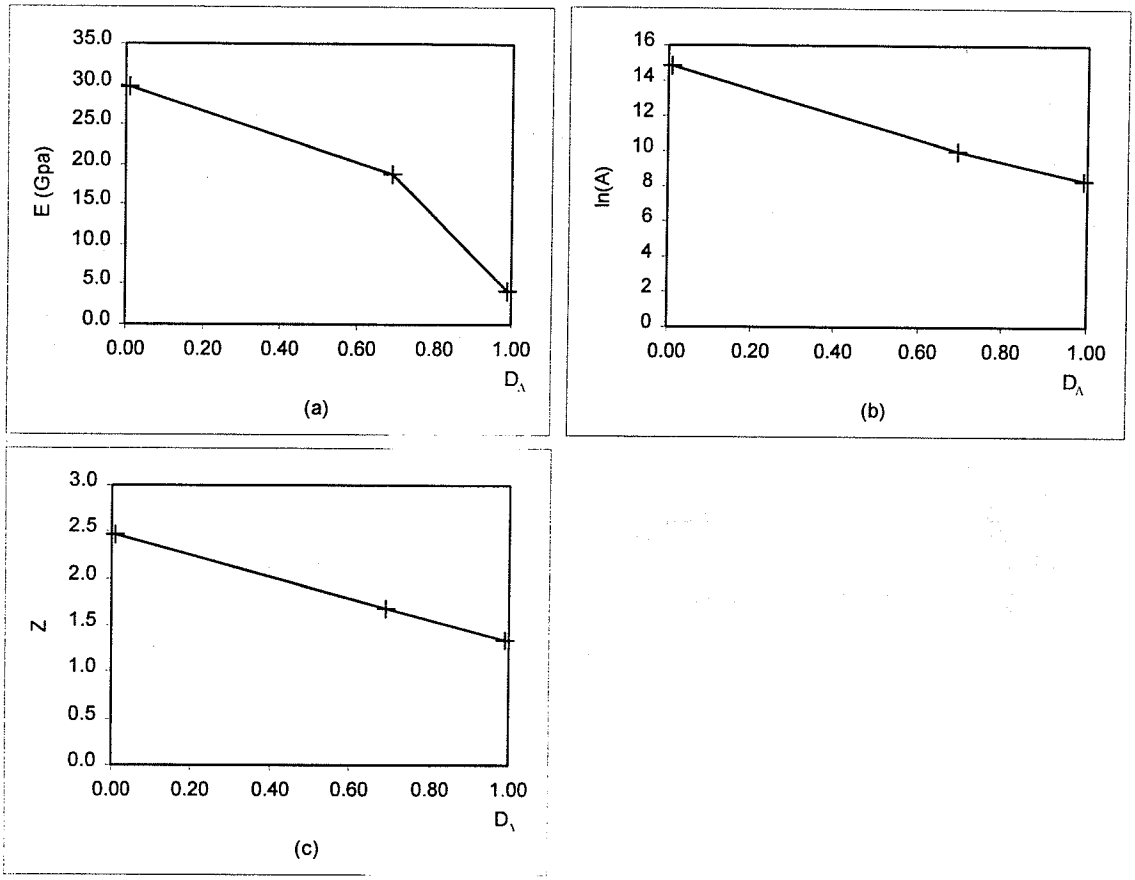

Fig. 13—Variation of mechanical parameters with disturbance (from Λ)

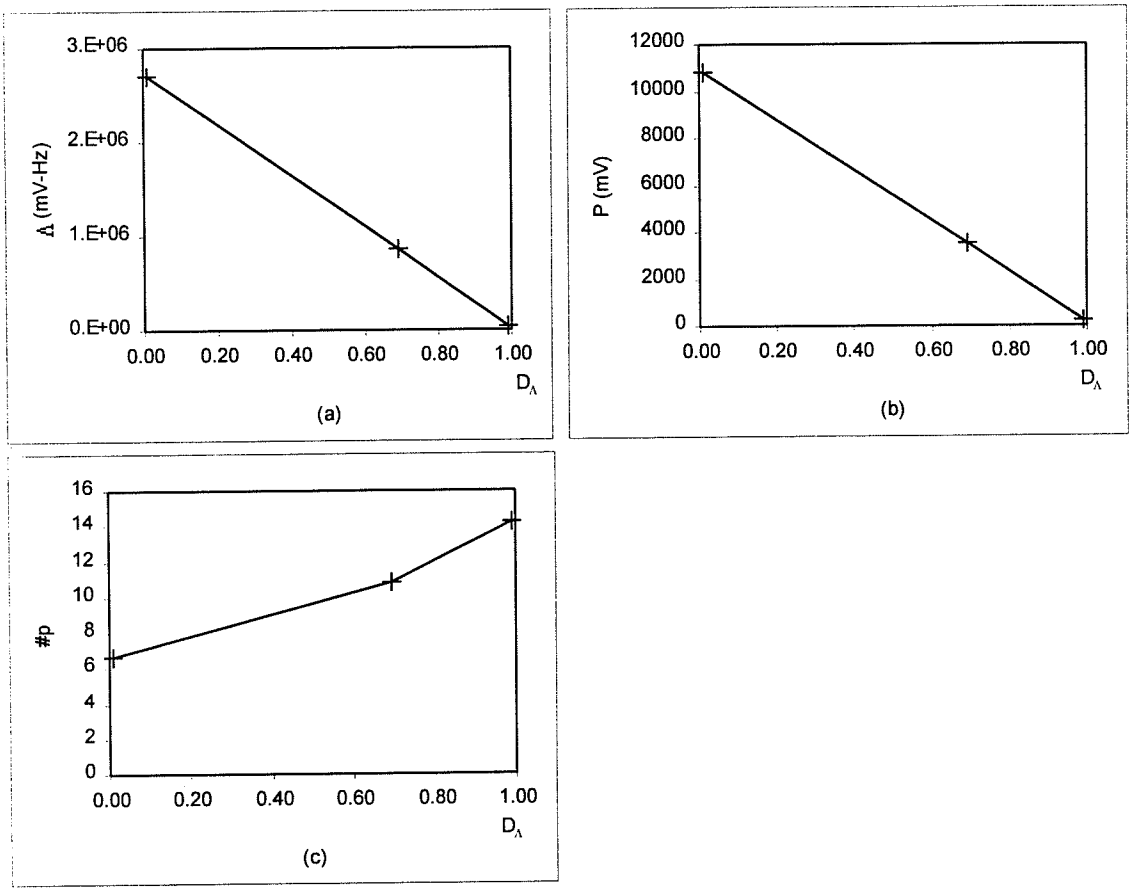

Fig. 14—Variation of NDT parameters with disturbance (from Λ)

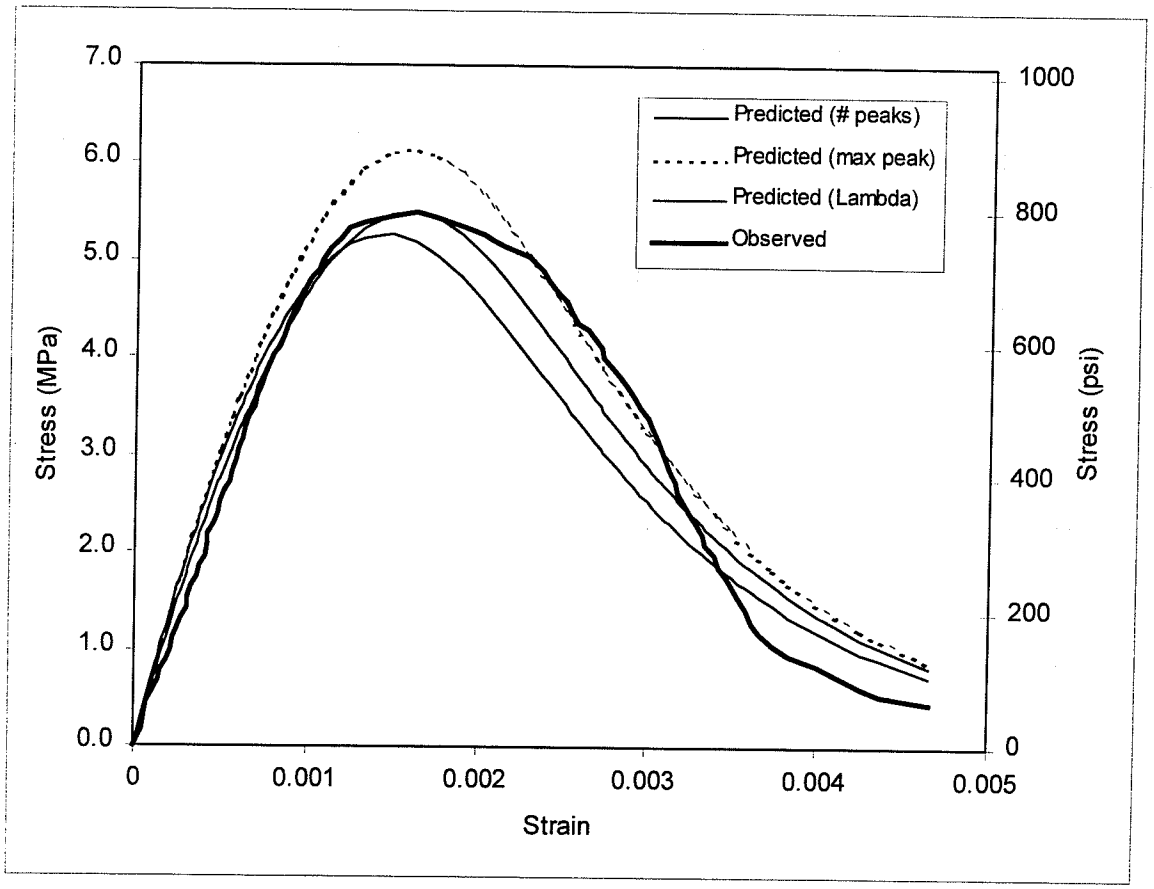

Fig. 15—Predicted vs. actual stress strain response for mortar mixture IV.

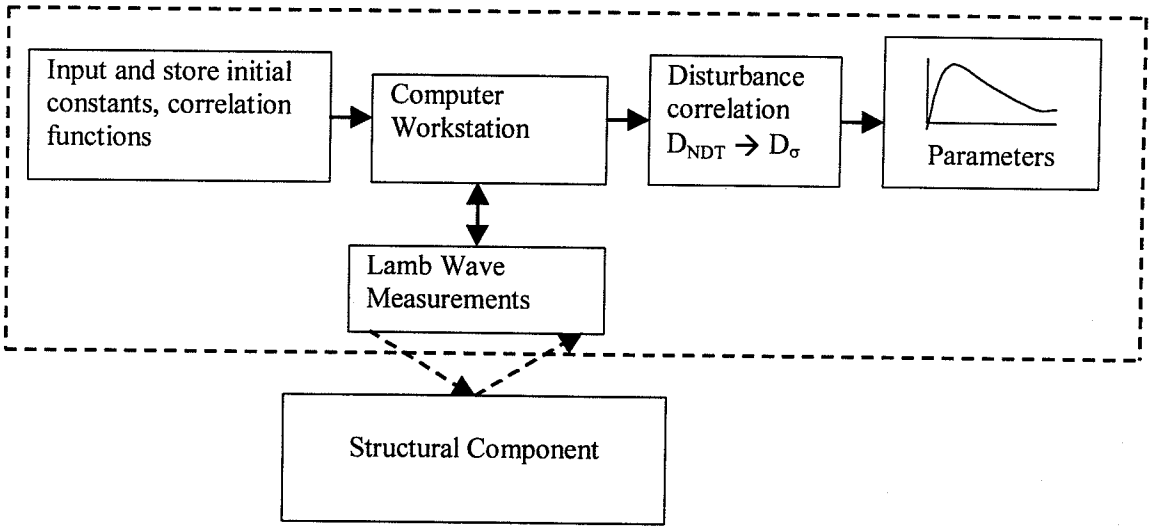

Fig. 16—Lamb Wave—DSC (LW-DSC) field equipment for predicting stress-strain response

Table 1—Mortar mix ratios

Mixture Set	water cement ratio	cement sand ratio
I	65%	1:12
II	65%	1:8
III	65%	1:4
IV	65%	1:10

Table 2—Test results for all samples

	σ_{peak}		E		nu	# peaks	Max peak	Λ	Z	A/1000	Ln(A)
	MPa	psi	GPa	ksi			(mV)	(mV-Hz)			
I-1	2.64	383	4.16	603	0.19	17	198	52394	1.095	0.8	6.737
I-2	2.67	387	3.18	461	0.20	13	220	52055	1.039	0.6	6.476
I-3	2.61	379	4.96	719	0.16	13	206	51909	1.526	10.7	9.277
I-4	2.78	403	4.67	677	0.18	18	184	31610	1.351	5.8	8.674
I-5	2.81	408	4.40	638	0.21	10	235	52699	1.693	29.2	10.282
Average I	**2.70**	**392**	**4.27**	**620**	**0.18**	**14.2**	**209**	**48133**	**1.341**		**8.289**
II-1	19.9	2888	16.2	2350	0.23	12	3791	1087770	1.474	9.3	9.143
II-2	20.3	2947	19.1	2771	0.16	10	3059	714872	1.587	11.2	9.323
II-3	18.1	2632	15.7	2270	0.16	10	4043	894944	1.180	1.4	7.217
II-4	24.2	3517	23.1	3346	0.16	12	3043	711410	2.598	3042.1	14.928
II-5	20.8	3018	20.0	2899	0.14	10	3656	933840	1.535	11.5	9.350
Average II	**20.7**	**3000**	**18.8**	**2727**	**0.17**	**10.8**	**3518**	**868567**	**1.67**		**9.99**
III-1	53.7	7791	28.9	4193	0.18	9	13524	3381408	2.432	1680.8	14.335
III-2			29.0	4208	0.18	6	11266	2852408			
III-3						6	10140	2501632			
III-4	51.4	7452	31.4	4547	0.18	5	7850	2201816	2.514	4150.6	15.239
III-5						7	11464	2619856			
Average III	**52.6**	**7622**	**29.8**	**4316**	**0.18**	**6.6**	**10849**	**2711424**	**2.473**		**14.787**
IV-1	5.68	824	7.44	1079		14	440	119091	1.220	2.4	7.780
IV-2	6.34	920	8.29	1203		12	758	142914	1.924	146.3	11.894
IV-3	5.90	856	7.06	1024		14	603	165728	1.291	2.9	7.975
IV-4	5.10	740	8.41	1219		16	1036	169968	1.068	0.7	6.487
IV-5	5.66	820	7.95	1153		12	1058	168606	1.331	4.0	8.298
Average IV	**5.74**	**832**	**7.83**	**1136**	**N/A**	**13.6**	**779**	**153261**	**1.367**		**8.49**

Table 3—Measured and predicted results for mixture IV

Mixture IV	σ_{peak}		E		ln(A)	Z
	Mpa	psi	Gpa	ksi		
measured	5.74	832	7.83	1136	8.490	1.367
predicted						
# peaks	5.07	736	7.21	1045	8.356	1.366
max peak	6.43	932	7.21	1045	8.489	1.391
Λ	5.80	841	6.47	938	8.404	1.377

REFERENCES

1. Jones, R., 1962, "Surface wave technique for measuring the elastic properties and thickness of roads: Theoretical development," British Journal of Applied Physics, **13**, pp. 21-29.
2. Heisley, J. S., Stokoe, K. H. III, and Meyer, A.H. 1983, "Moduli of pavement systems from analysis of surface waves," Transp. Res. Record, 852, TRB, Washington, DC, 22-31.
3. Ioannides, A. M. 1990, "Dimensional analysis in NDT rigid pavement evaluation," J. of Transportation Engineering, ASCE, 116(1), 23-36.
4. Krause, M., Wiggenhauser, H., Barmann, O., Langenberg, K., Frielinghaus, R., Wollbold, F., Schichert, M., 1995, "Comparison of Pulse-Echo Methods for Testing Concrete", Proceedings of the International Symposium on Nondestructive Testing in Civil Engineering (NDT-CE), **1**, Berlin, Germany, DGZFP, pp. 281-296.
5. Malhotra, V. M., and Carino, N. J., 1991, "CRC Handbook on nondestructive Testing of Concrete", CRC Press.
6. Pessiki, S. and Johnson, M., 1994, "Nondestructive Determination of Concrete Strength in Plate Structures by the Impact Echo Method", Review of Progress in Quantitative Nondestructive Evaluation, **13**, pp. 2139-2146.
7. Sansalone, M. J., and Strett, W. B., 1997, "Impact-echo: Nondestructive Evaluation of Concrete and Masonry", Bullbrier Press.
8. Nagy, P. B., Adler, L., Mih, D., and Sheppard, W., 1989, "Single mode Lamb wave inspection of composite laminates," Review of Progress in Quantitative NDE, D.O. Thompson and D. E. Chimenti (eds), plenum Press, New York, **8B**, pp. 1535-1542.

9. R. W. Whitcomb, L. Jacobs, and L. Aref 1992, "Quantitative Ultrasonic Evaluation of Concrete" Proceedings of the International Conference on Nondestructive Testing of Concrete in the infrastructure, pp 238-255.
10. Jung, Y. C., Na, W. B., Kundu, T. and Ehsani, M. R., 2000, "Damage Detection in Concrete Using Lamb Waves", Nondestructive Evaluation of Highways, Utilities, and Pipelines IV, Ed. A. E. Aktan and S. R. Gosselin, Proc. Of SPIE NDE 2000, March 5-9, 2000, Newport Beach, California, **3995**,pp.448-458.
11. Kundu, T., Ehsani, M., Maslov, K. I. and Guo, D., 1999, "C-Scan and L-Scan Generated Images of the Concrete/GFRP Composite Interface", NDT&E International, **32**, pp.61-69.
12. Na, W. B., Kundu, T. and Ehsani, M. R., 2000, "Ultrasonic Guided Waves for Steel Bar-Concrete Interface Inspection", Materials Evaluation, in press, 2001.
13. Popovics, J. S., 1994, "Some Theoretical and Experimental Aspects of the Use of Guided Waves for the Nondestructive Evaluation of Concrete", Ph.D. Dissertation, The Pennsylvania State University, University Park, PA.
14. Desai, C. S. 2001, "Mechanics of Materials and Interfaces: The Disturbed State Concept," CRC Press, Boca Raton, Florida.
15. Schmerr, L. W. 1998, "Fundamentals of Ultrasonic Nondestructive Evaluation," Plenum Press, New York and London.
16. Mindlin, R. D., 1960, "Waves and Vibrations in Isotropic Elastic Plates", in Structural Mechanics (J. N. Goodier and N. J. Hoff, eds.), Pergamon, NY.
17. Kachanov, L. M., 1986, "Introduction to Continuum Damage Mechanics", Martinus Nijhuft Publishers, Dordrecht, The Netherlands.
18. Schickert, G. and Wiggenhauser, H., 1995, "Comparison of DIN/ISO 8047 (Entwurf) to Several Standards on Determination of Ultrasonic Pulse Velocity in Concrete" International Symposium on Non-Destructive Testing in Civil

Engineering (NDT-CE) Sept. 26-28, 1995, Berlin. Germany Proceedings **1** Lectures **2**, p. 1346.

19. Jung, Y.C., Kundu, T and Ehsani, M. R., "Internal Discontinuity Detection in Concrete by Lamb Waves", Materials Evaluation, **59**(3), pp. 418-423, 2001.
20. Na, W. B., Kundu, T. and Ehsani, M. R., 2001, "Lamb Waves for Detecting Delamination between Steel Bars and Concrete", Journal of Computer-Aided Civil and Infrastructure Engineering, in press, 2001.
21. Desai, C. S., and Toth, J. 1996, "Disturbed state constitutive modeling based on stress-strain and nondestructive behavior," Int. J. solids and Structures, 33, 11, pp. 1619-1650.

APPENDIX 1: DETAILS OF MECHANICAL AND NONDESTRUCTIVE TESTING

Table 1-I— Test results for samples of mortar mixture I

Sample	Max Stress (psi)	E (ksi)	nu	ln(A)	Z	# Peaks	Max Peak	Lambda
I-1	383	603	0.19	6.74	1.10	17	198	52394
I-2	387	461	0.20	6.48	1.04	13	220	52055
I-3	379	719	0.16	9.28	1.53	13	206	51909
I-4	403	677	0.18	8.67	1.35	18	184	31610
I-5	408	638	0.21	10.28	1.69	10	235	52699
Average	**392**	**620**	**0.18**	**8.29**	**1.34**	**14.2**	**209**	**48133**

Table 1-II— Test results for samples of mortar mixture II

Sample	Max Stress (psi)	E (ksi)	nu	ln(A)	Z	# Peaks	Max Peak	Lambda
II-1	2888	2350	0.23	9.14	1.47	12	3791	1087770
II-2	2947	2771	0.16	9.32	1.59	10	3059	714872
II-3	2632	2270	0.16	7.22	1.18	10	4043	894944
II-4	3517	3346	0.16	14.93	2.60	12	3043	711410
II-5	3018	2899	0.14	9.35	1.54	10	3656	933840
Average	**3000**	**2727**	**0.17**	**9.99**	**1.67**	**10.8**	**3518**	**868567**

Table 1-III— Test results for samples of mortar mixture III

Sample	Max Stress (psi)	E (ksi)	nu	ln(A)	Z	# Peaks	Max Peak	Lambda
III-1	7791	4193	0.18	14.33	2.43	9	13524	3381408
III-2	*	4208	0.18	*	*	6	11266	2852408
III-3	*	*	*	*	*	6	10140	2501632
III-4	7452	4547	0.18	15.24	2.51	5	7850	2201816
III-5	*	*	*	*	*	7	11464	2619856
Average	**7622**	**4316**	**0.18**	**14.79**	**2.47**	**6.6**	**10849**	**2711424**

*Only Samples 1 and 4 were loaded to failure. The others could not be broken (too strong). Elastic properties could be determined from sample 2, but 3 and 5 had to be cut thinner and then they buckled rather than crushing.

Table 1-IV— Test results for samples of mortar mixture IV

Sample	Max Stress (psi)	E (ksi)	nu	ln(A)	Z	# Peaks	Max Peak	Lambda
IV-1	824	1079	N/A	7.78	1.22	14	440	119091
IV-2	920	1203	N/A	11.89	1.92	12	758	142914
IV-3	856	1024	N/A	7.97	1.29	14	603	165728
IV-4	740	1219	N/A	6.49	1.07	16	1036	169968
IV-5	820	1153	N/A	8.30	1.33	12	1058	168606
Average	**832**	**1136**	**N/A**	**8.49**	**1.37**	**13.6**	**779**	**153261**

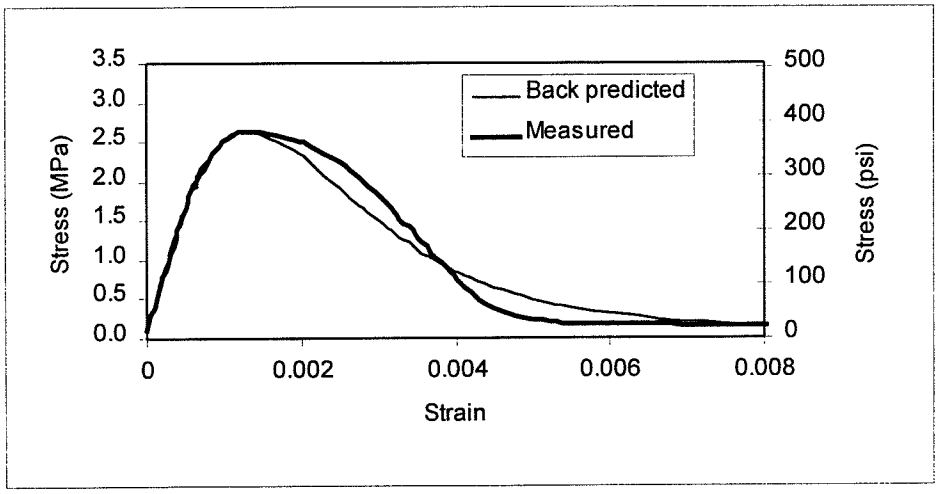

Fig. 1-I1 (a)—Measured and back predicted stress strain response of sample I-1

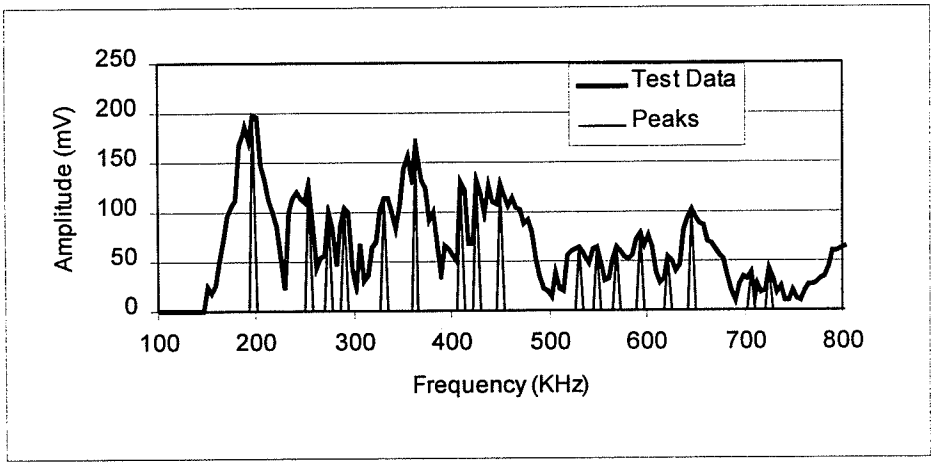

Fig. 1-I1 (b)—V(f) curve for sample I-1

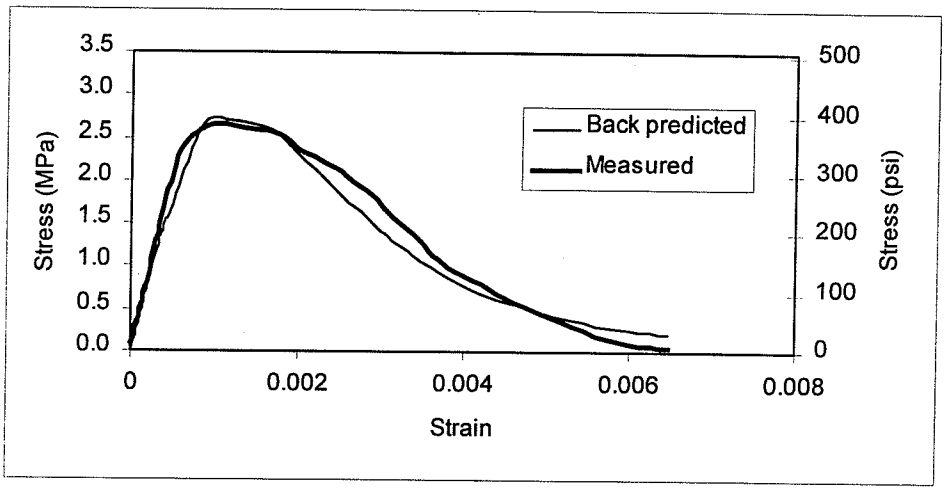

Fig. 1-I2 (a)—Measured and back predicted stress strain response of sample I-2

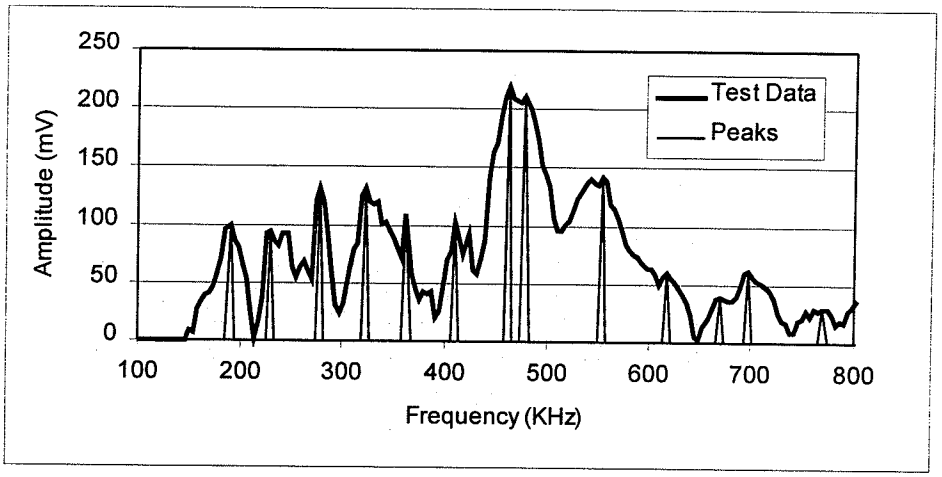

Fig. 1-I2 (b)—V(f) curve for sample I-2

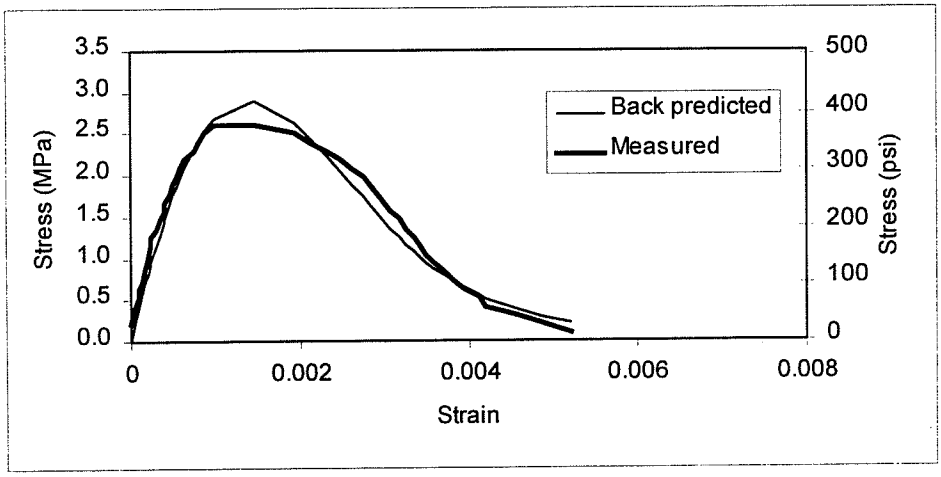

Fig. 1-I3 (a)—Measured and back predicted stress strain response of sample I-3

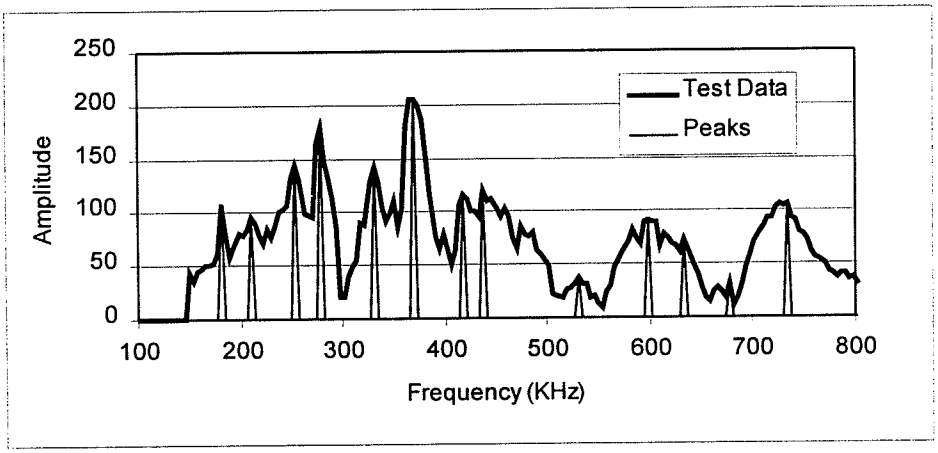

Fig. 1-I3 (b)—V(f) curve for sample I-3

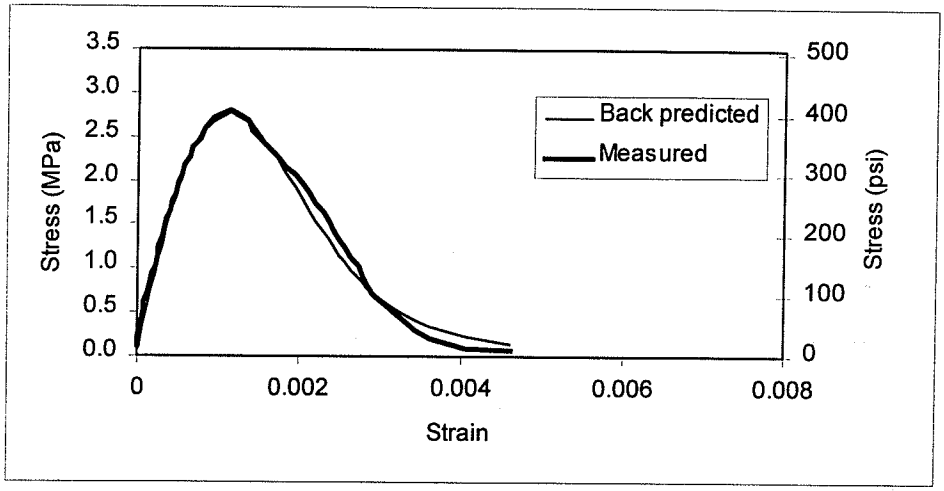

Fig. 1-I4 (a)—Measured and back predicted stress strain response of sample I-4

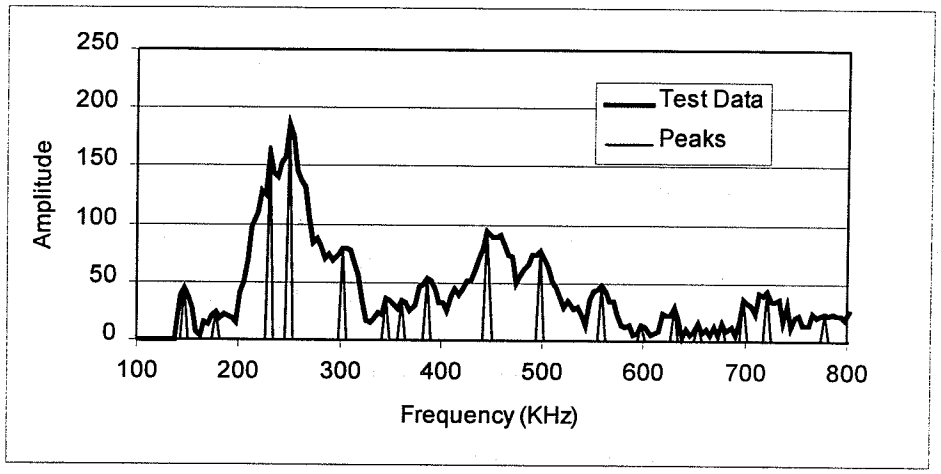

Fig. 1-I4 (b)—V(f) curve for sample I-4

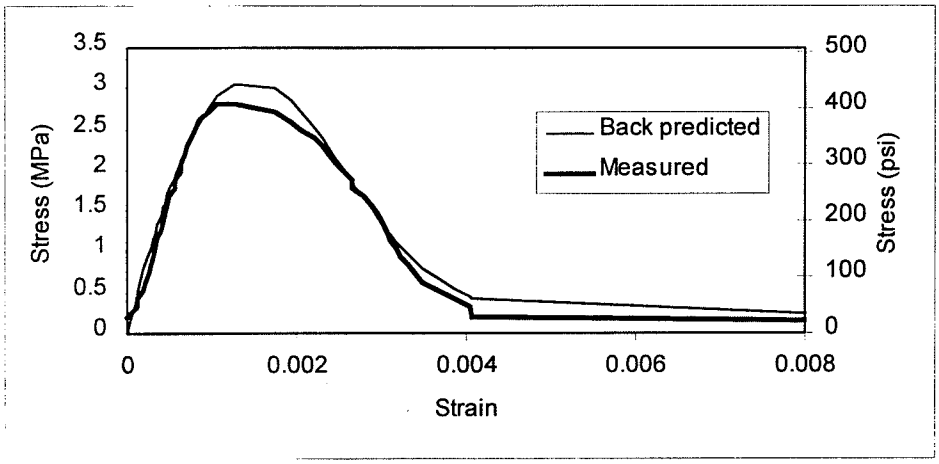

Fig. 1-I5 (a) – Measured and back predicted stress strain response of sample I-5

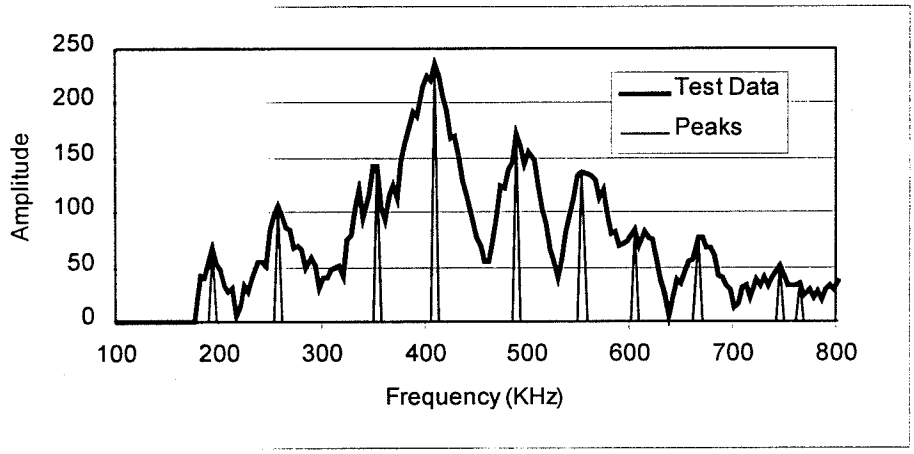

Fig. 1-I5 (b)—V(f) curve for sample I-5

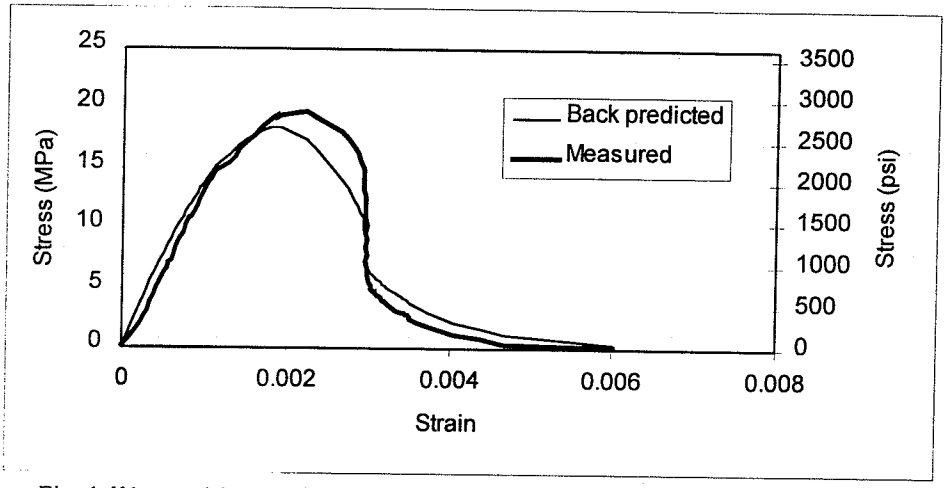

Fig. 1-III (a)—Measured and back predicted stress strain response of sample II-1

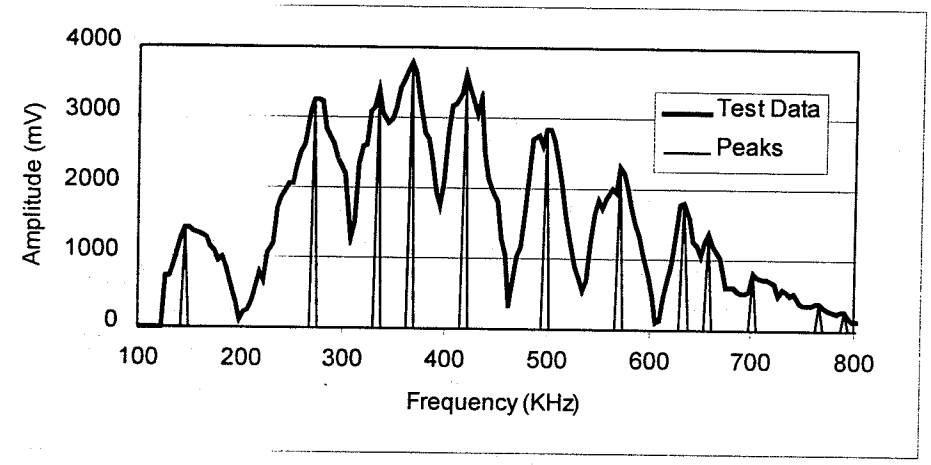

Fig. 1-III (b)—V(f) curve for sample II-1

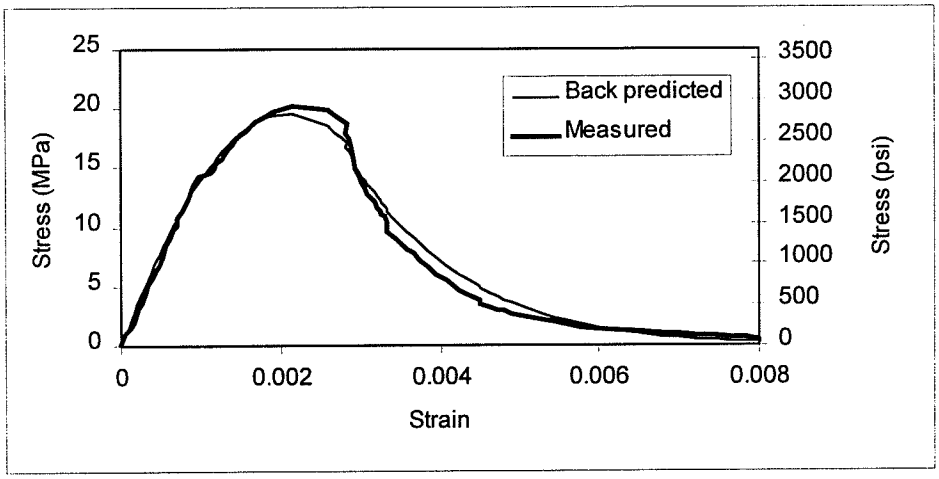

Fig. 1-II2 (a)—Measured and back predicted stress strain response of sample II-2

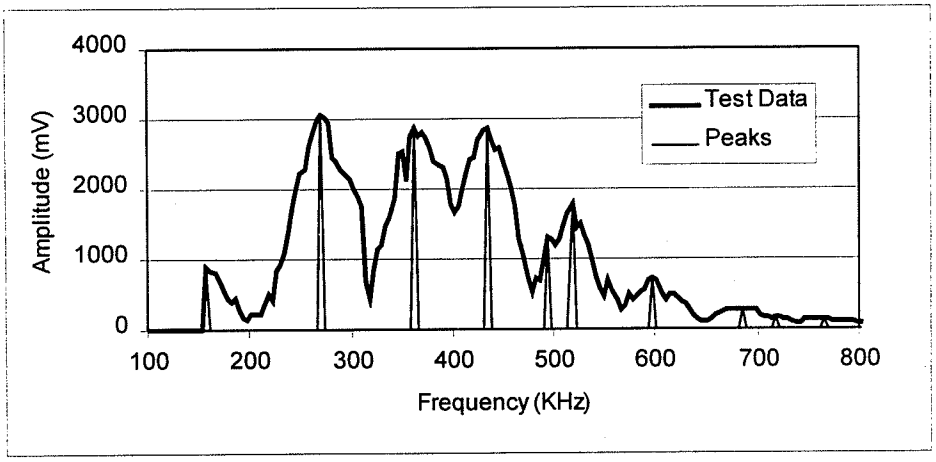

Fig. 1-II2 (b)—V(f) curve for sample II-2

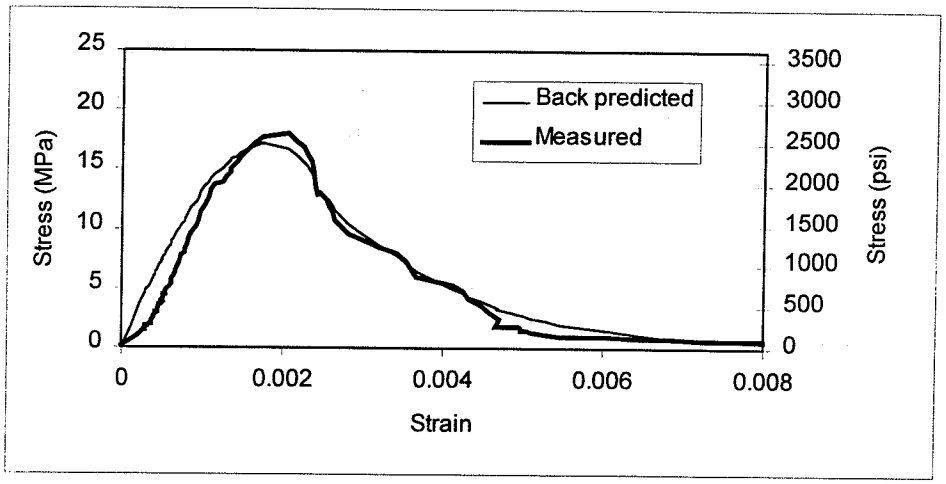

Fig. 1-II3 (a)—Measured and back predicted stress strain response of sample II-3

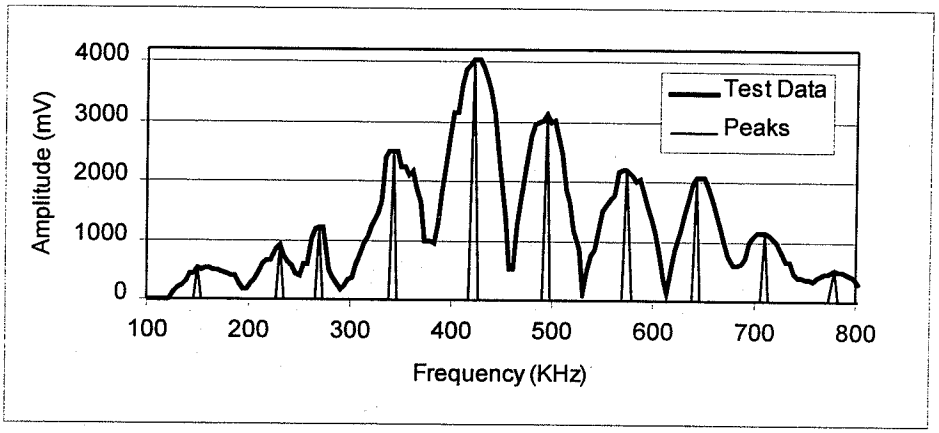

Fig. 1-II3 (b)—V(f) curve for sample II-3

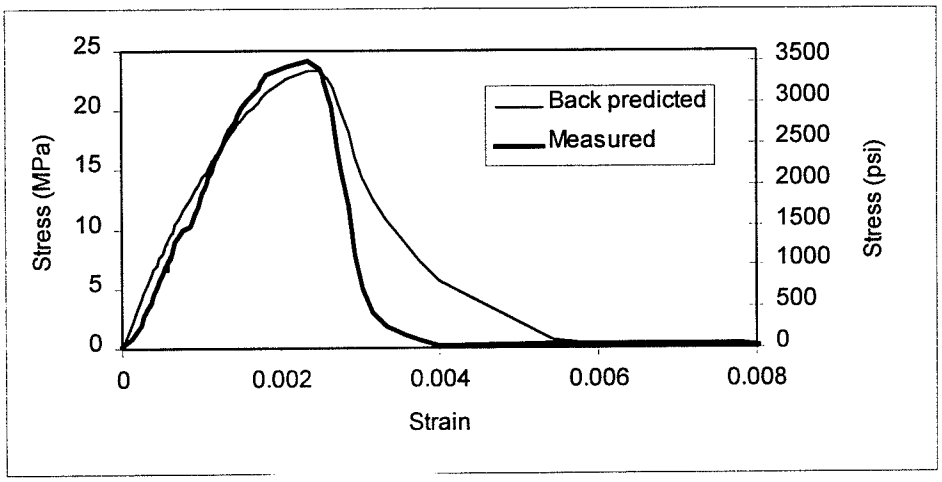

Fig. 1-II4 (a)—Measured and back predicted stress strain response of sample II-4

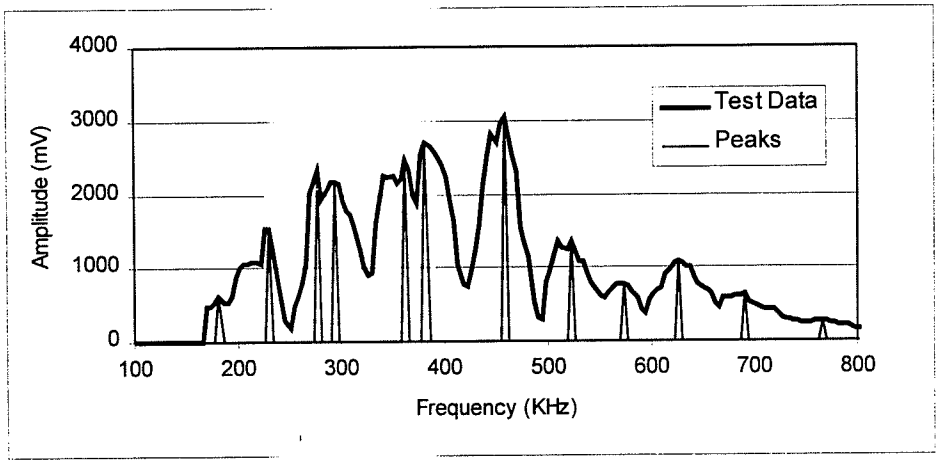

Fig. 1-II4 (b)—V(f) curve for sample II-4

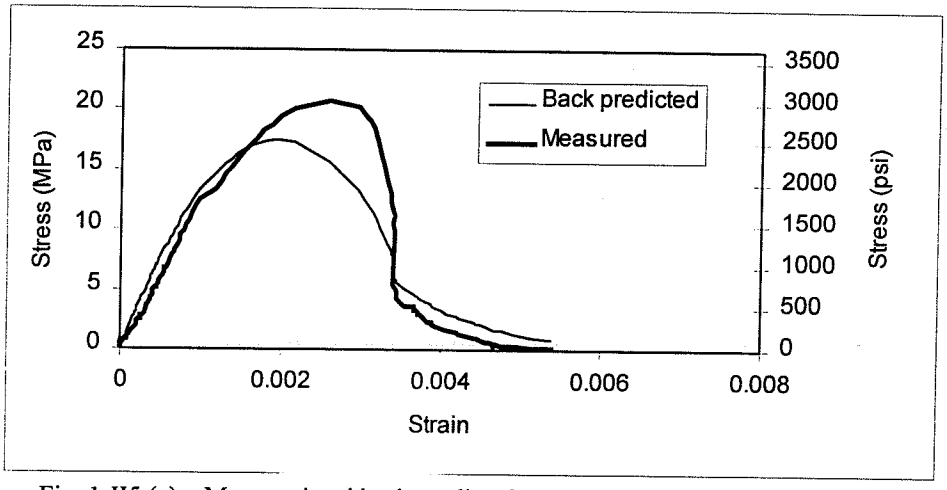

Fig. 1-II5 (a)—Measured and back predicted stress strain response of sample II-5

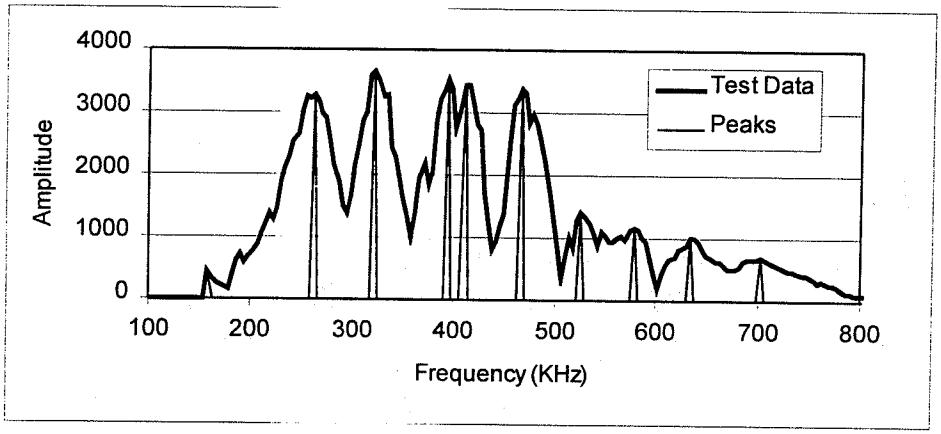

Fig. 1-II5 (b)—V(f) curve for sample II-5

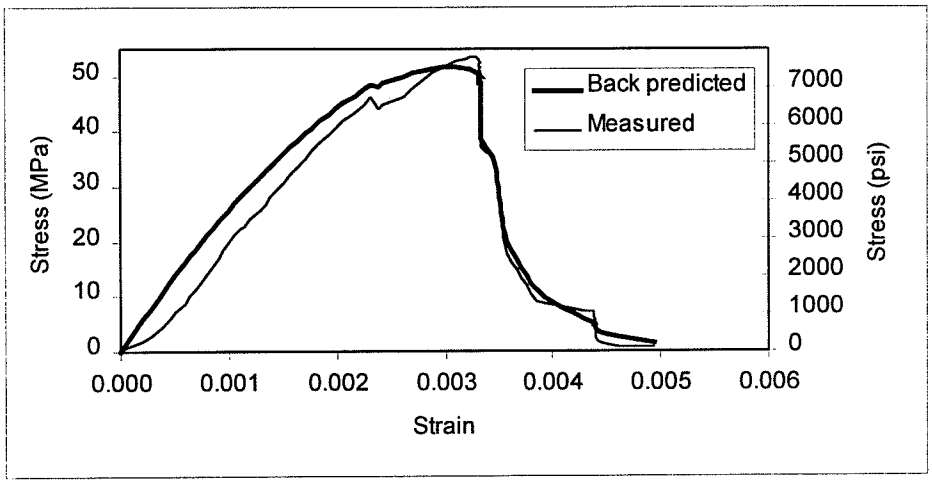

Fig. 1-III1 (a)—Measured and back predicted stress strain response of sample III-1

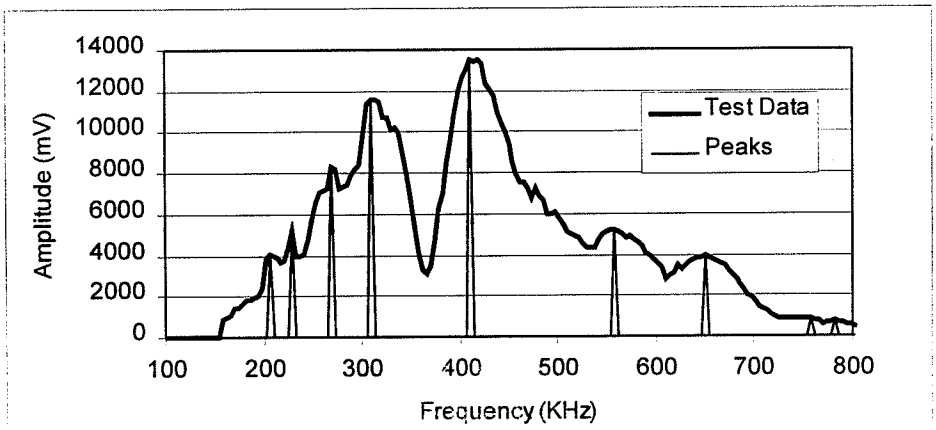

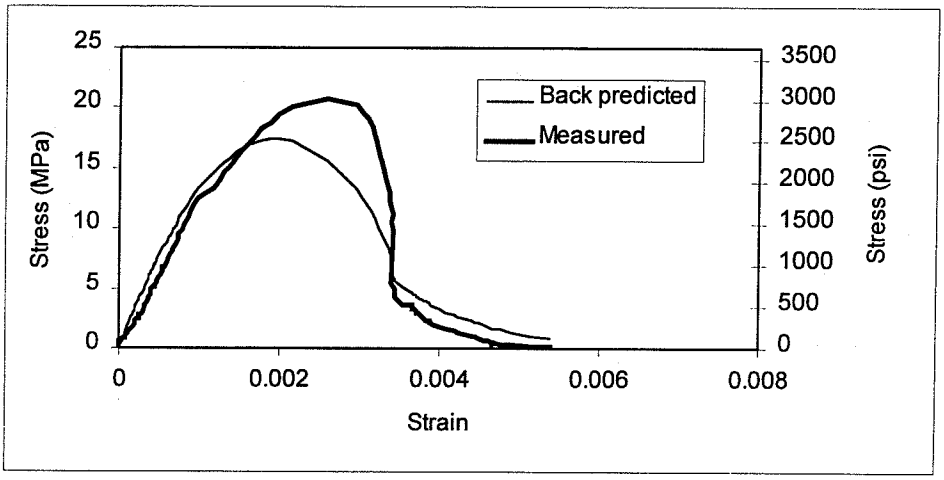

Fig. 1-II5 (a)—Measured and back predicted stress strain response of sample II-5

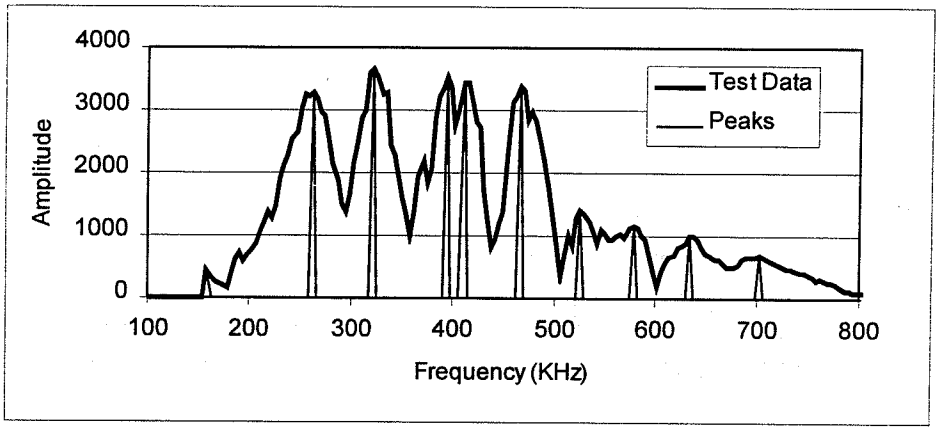

Fig. 1-II5 (b)—V(f) curve for sample II-5

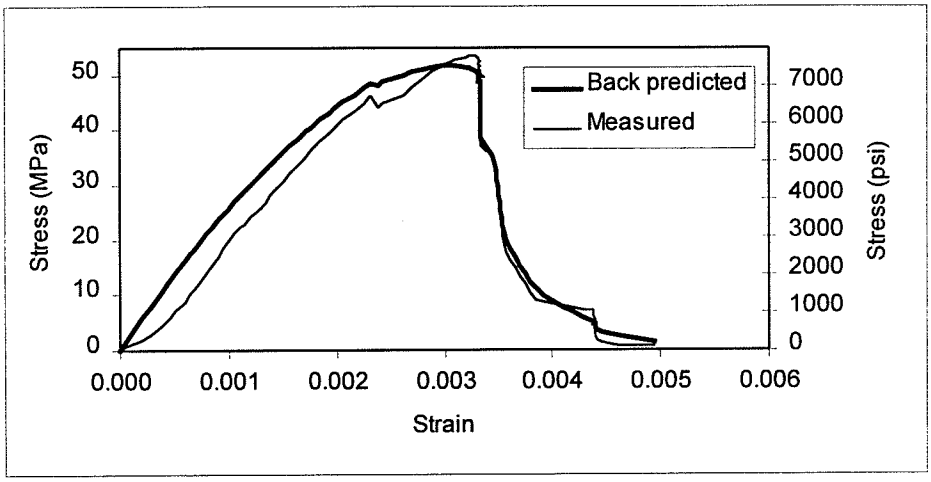

Fig. 1-III1 (a)—Measured and back predicted stress strain response of sample III-1

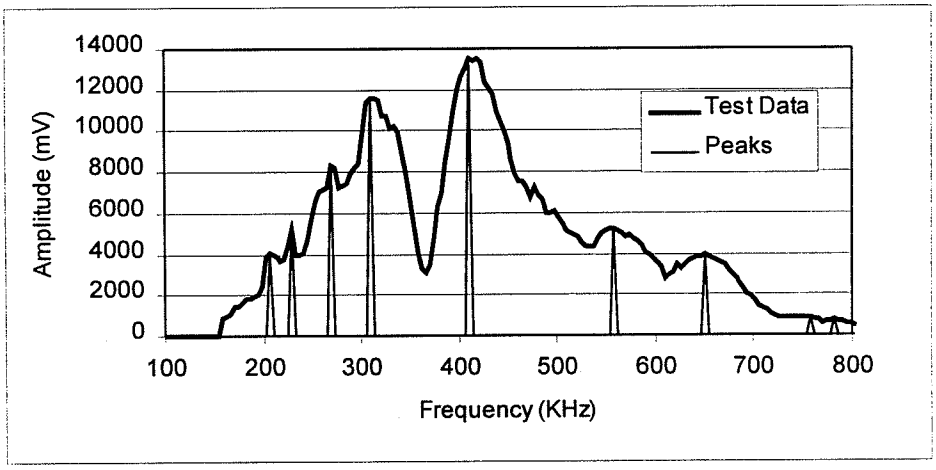

Fig. 1-III1 (b)—V(f) curve for sample III-1

Stress strain data not available for sample III-2—see Table 1-III

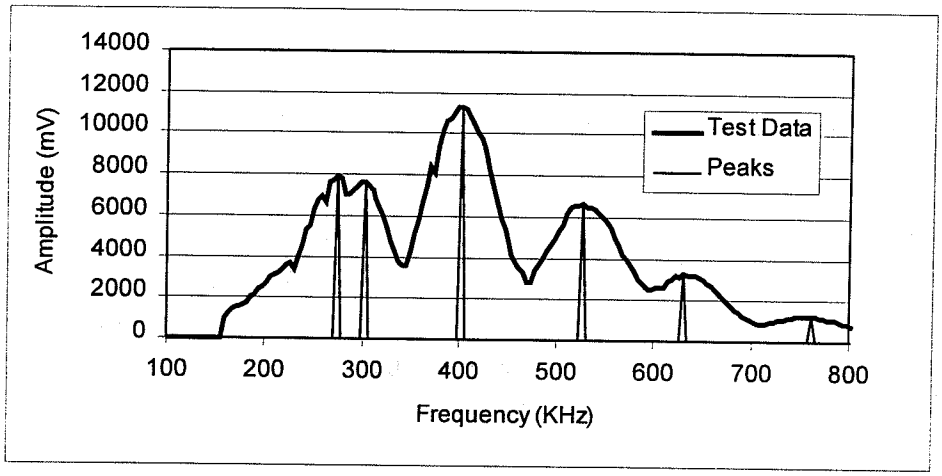

Fig. 1-III2 (b)—V(f) curve for sample III-2

Stress strain data not available for sample III-3—see Table 1-III

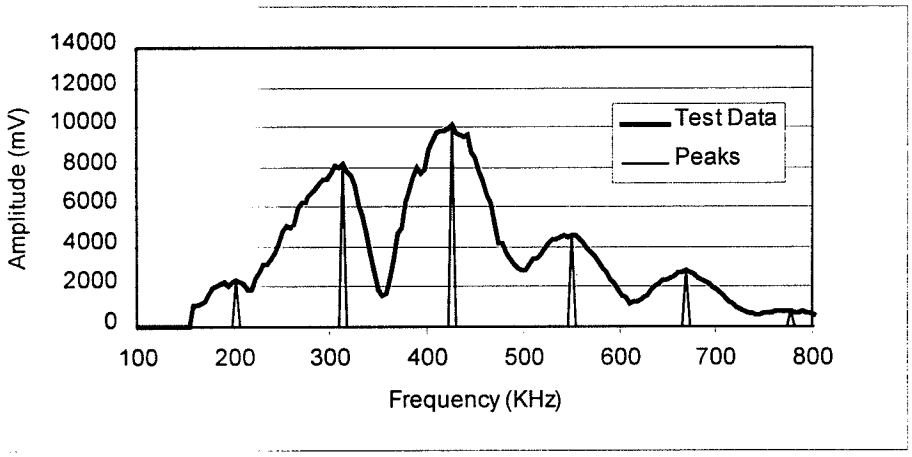

Fig. 1-III3 (b)—V(f) curve for sample III-3

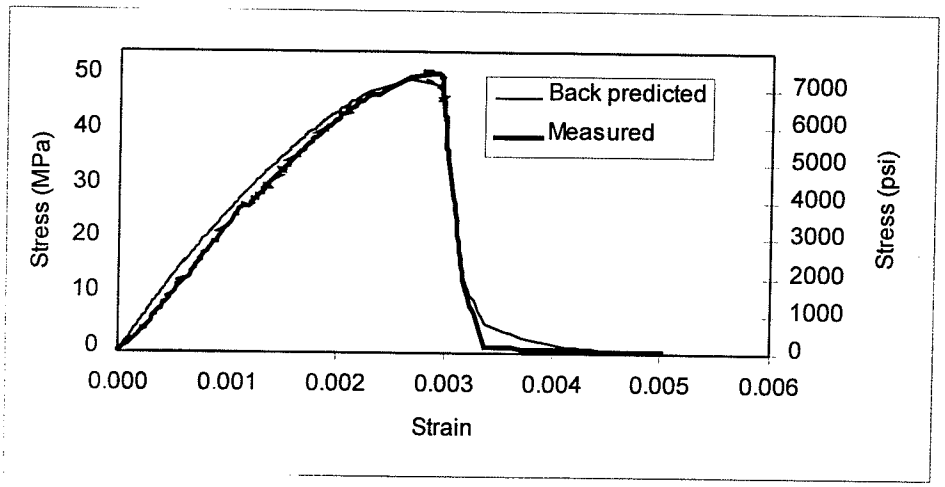

Fig. 1-III4 (a)—Measured and back predicted stress strain response of sample III-4

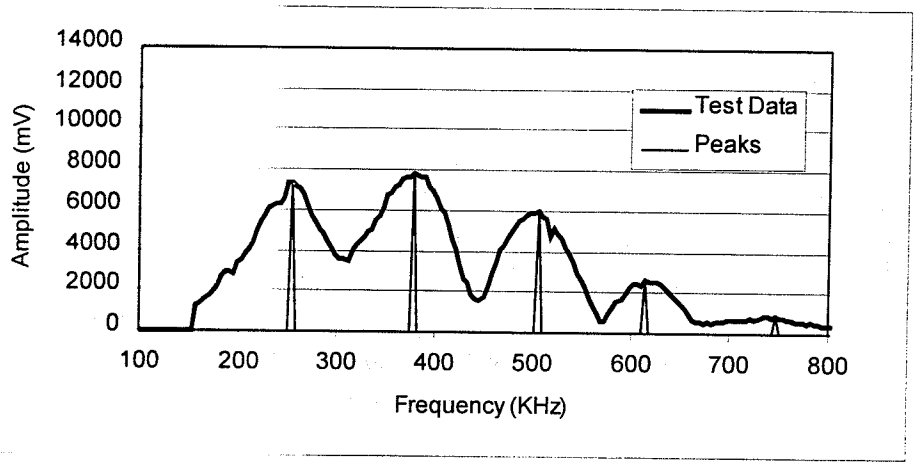

Fig. 1-III4 (b)—V(f) curve for sample III-4

Stress strain data not available for sample III-5—see Table 1-III

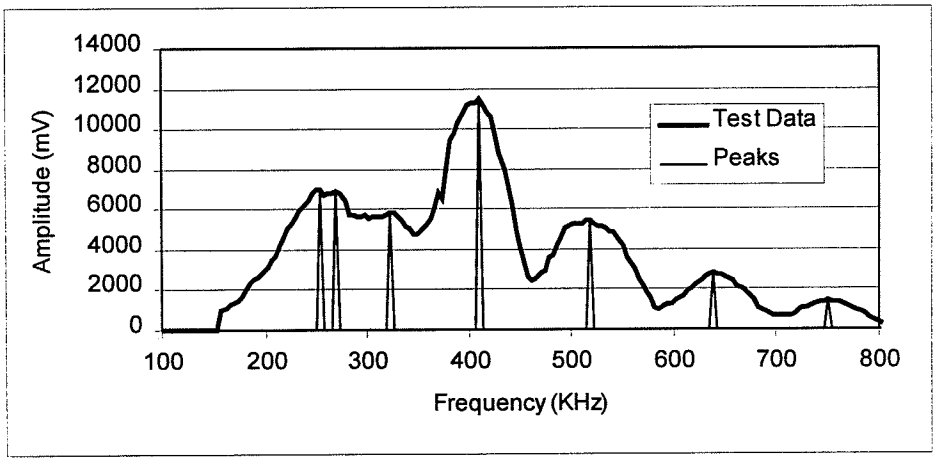

Fig. 1-III5 (b)—V(f) curve for sample III-5

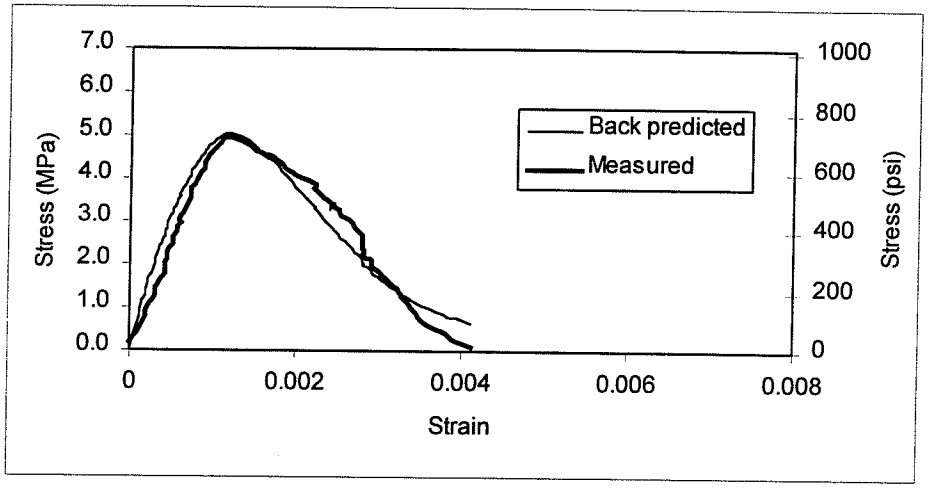

Fig. 1-IV1 (a)—Measured and back predicted stress strain response of sample IV-1

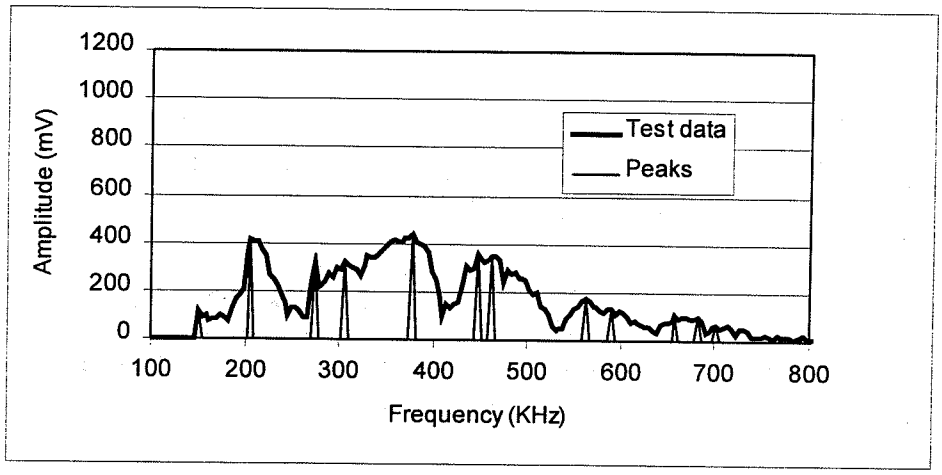

Fig. 1-IV1 (b)—V(f) curve for sample IV-1

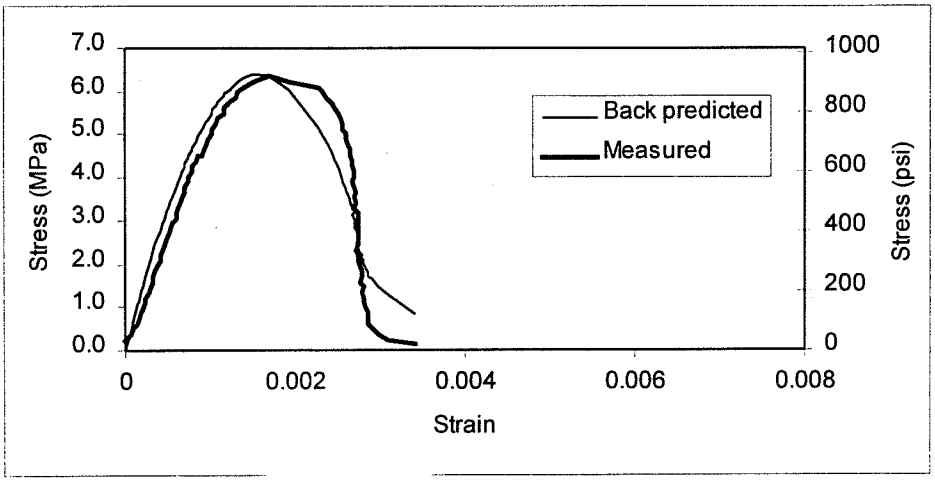

Fig. 1-IV2 (a)—Measured and back predicted stress strain response of sample IV-2

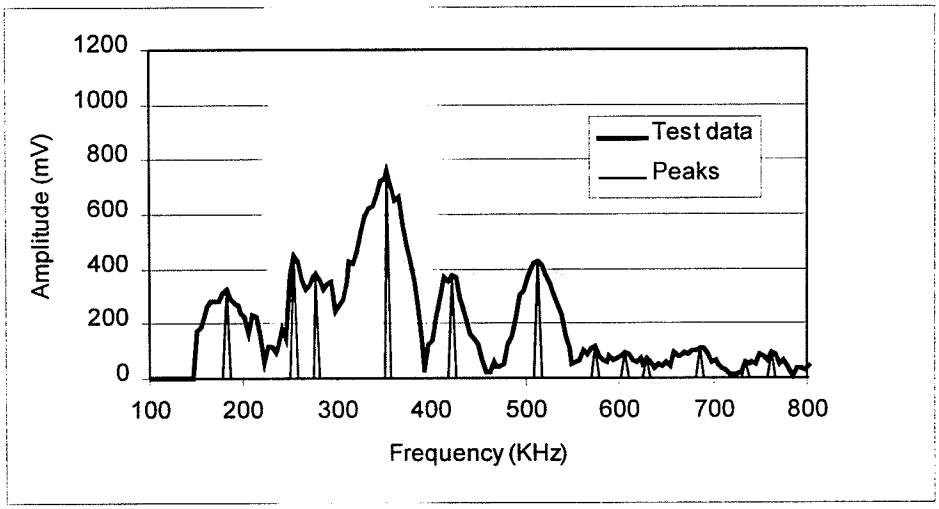

Fig. 1-IV2 (b)—V(f) curve for sample IV-2

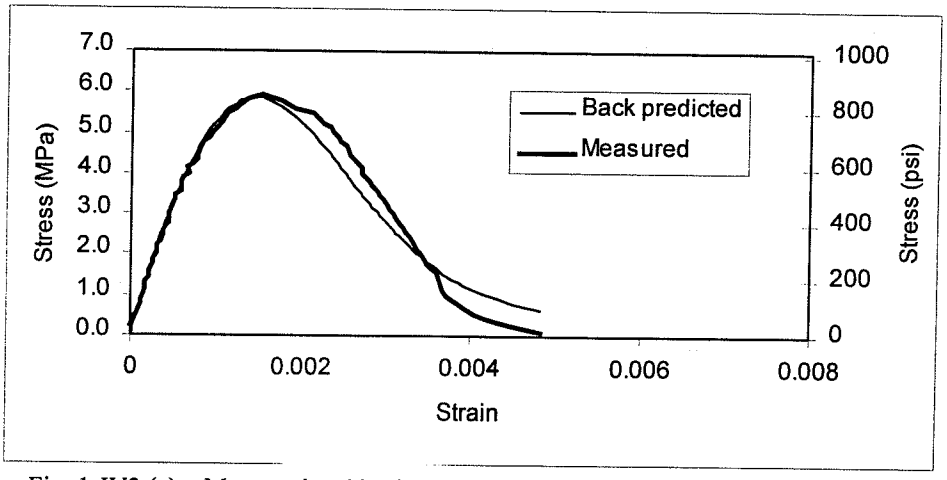

Fig. 1-IV3 (a)—Measured and back predicted stress strain response of sample IV-3

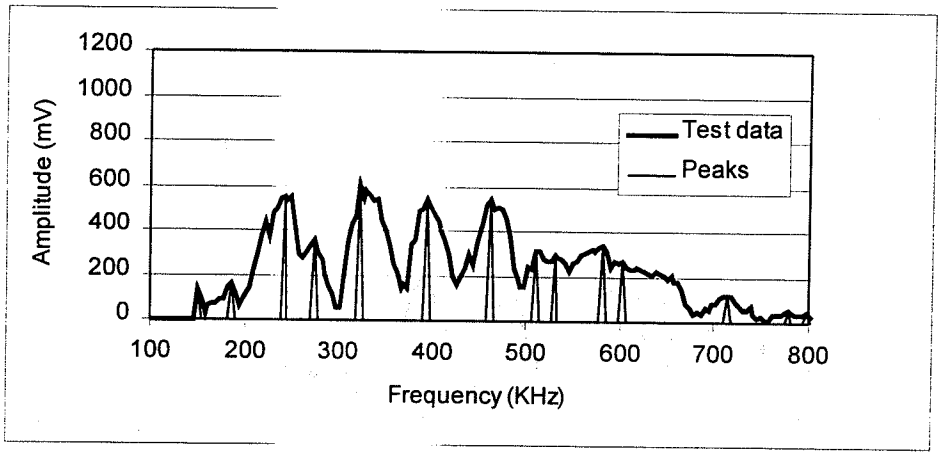

Fig. 1-IV3 (b)—V(f) curve for sample IV-3

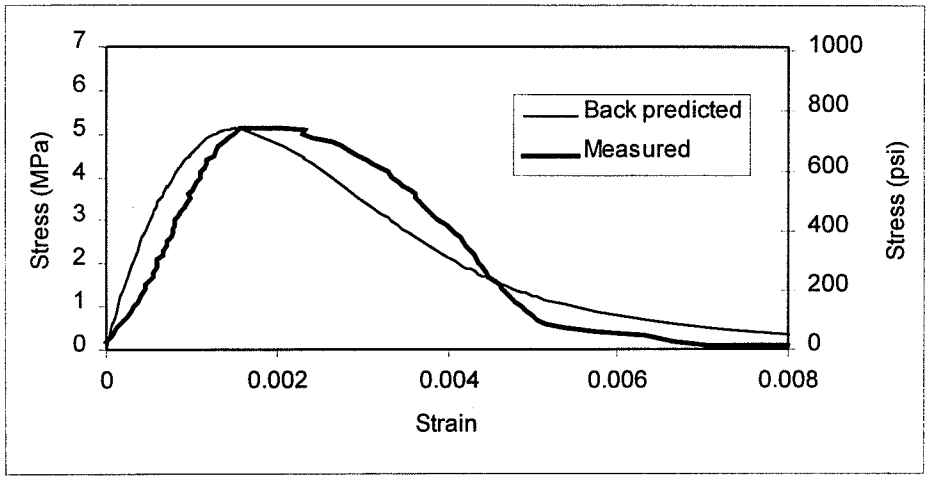

Fig. 1-IV4 (a)—Measured and back predicted stress strain response of sample IV-4

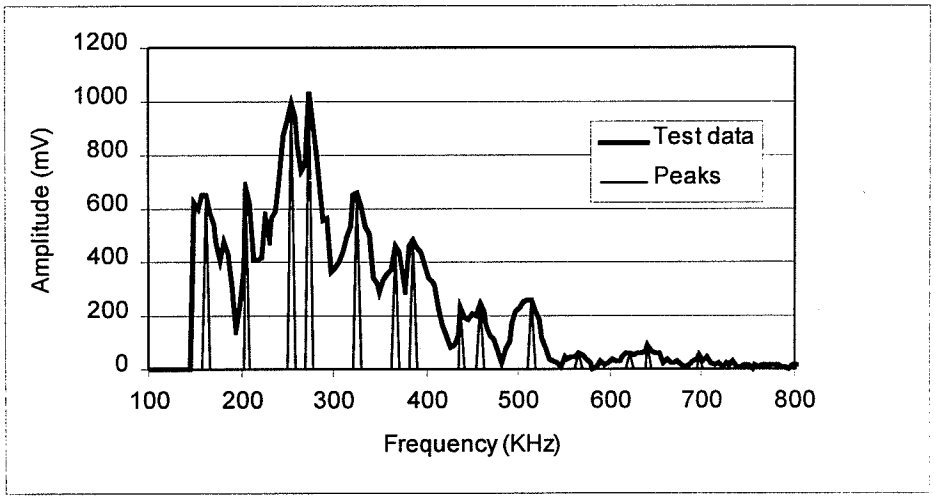

Fig. 1-IV4 (b)—V(f) curve for sample IV-4

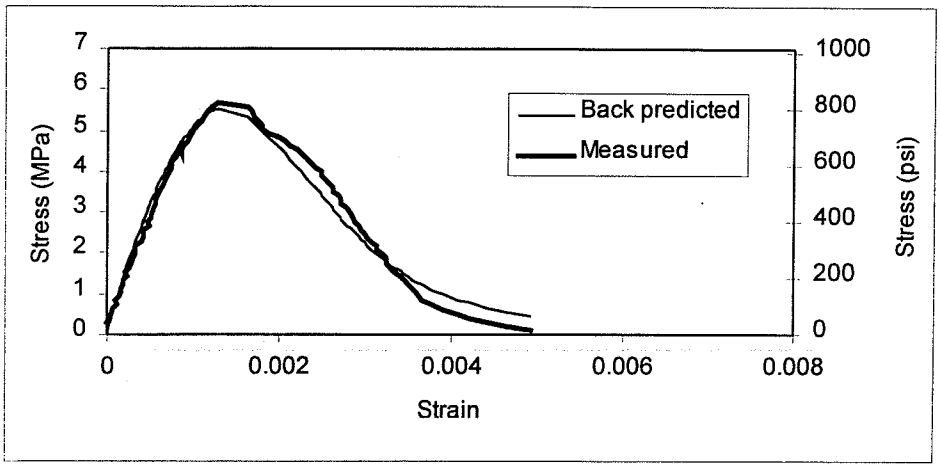

Fig. 1-IV5 (a)—Measured and back predicted stress strain response of sample IV-5

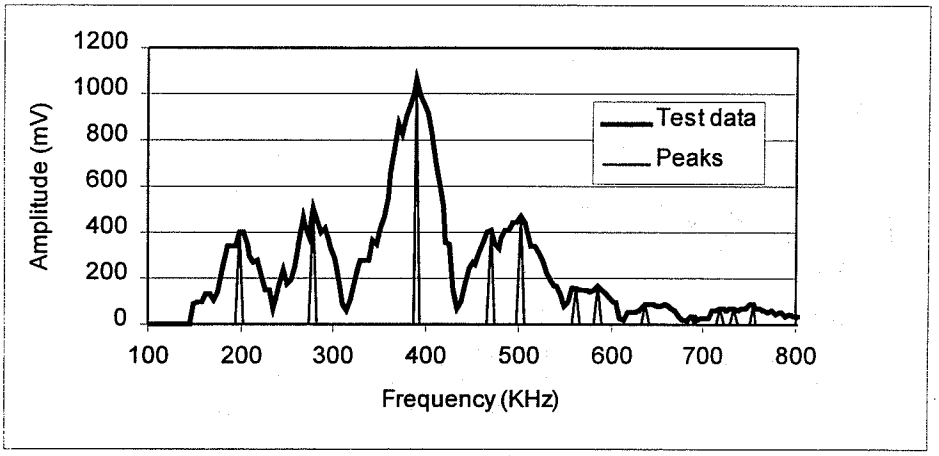

Fig. 1-IV5 (b)—V(f) curve for sample IV-5